System Identification of the Vincent Thomas Suspension Bridge using Earthquake Records

by

Andrew W. Smyth
Assistant Professor
School of Engineering & Applied Science
Columbia University
New York, New York 10027-6699

Jin-Song Pei
Graduate Student
School of Engineering & Applied Science
Columbia University
New York, New York 10027-6699

Sami F. Masri
Professor
Dept. of Civil Engineering
University of Southern California
Los Angeles, CA 90089-2531

Reprint from an article which appeared in

International Journal of Earthquake Engineering & Structural Dynamics (2003)
Vol. 32, pages 339-367

13 August 2004 16:49
"VTB˙Smyth etal˙reprint"

System Identification of the Vincent Thomas Suspension Bridge using Earthquake Records

Abstract

Contents

1 INTRODUCTION **1**
1.1 Motivation and Technical Challenges 1
1.2 Scope 3

2 VINCENT THOMAS BRIDGE AND ITS DYNAMIC MONITORING SYSTEM **3**
2.1 Vincent Thomas Bridge and Sensor Array 3
2.2 Earthquake Response Data Sets 4

3 FORMULATION OF TIME-DOMAIN IDENTIFICATION APPROACH **5**
3.1 Overview of time-domain identification approach 5
3.2 Identification of nonlinear residual terms 7
3.3 Identification of modal frequencies, damping coefficients and mode shapes 7

4 LINEAR IDENTIFICATION RESULTS **8**
4.1 Shifted window identification for nonstationary process analysis 9
4.2 Identified modal frequencies and damping ratios 10
4.3 Identified complex mode shapes and their physical interpretations 11
4.4 Identified results of $^{3}\mathbf{A}$ matrix 12
4.5 Comparison of identified results of the 1987 Whittier and 1994 Northridge earthquakes . . . 13

5 NONLINEAR IDENTIFICATION RESULTS **14**

6 DISCUSSION **14**
6.1 Preliminary data processing 15
6.2 Comparison with other identification methodologies 15

7 CONCLUSION **16**

8 ACKNOWLEDGMENTS **17**

9 REFERENCES **18**

System Identification of the Vincent Thomas Suspension Bridge using Earthquake Records

ABSTRACT

The Vincent Thomas Bridge in the Los Angeles metropolitan area, is a critical artery for commercial traffic flow in and out of the Los Angeles Harbor, and is at risk in the seismically active Southern California region, particularly because it straddles the Palos Verdes fault zone. A combination of linear and nonlinear system identification techniques is employed to obtain a complete reduced-order, multi-input-multi-output (MIMO) dynamic model of the Vincent Thomas Bridge based on the dynamic response of the structure to the 1987 Whittier and 1994 Northridge earthquakes.

Starting with the available acceleration measurements (which consists of 15 accelerometers on the bridge structure and 10 accelerometers at various locations on its base), an efficient least-squares-based time-domain identification procedure is applied to the data set to develop a reduced-order, equivalent linear, multi-degree-of-freedom model. Although not the main focus of this study, the linear system identification method is also combined with a nonparametric identification technique, to generate a reduced-order nonlinear mathematical model suitable for use in subsequent studies to predict, with good fidelity, the total response of the bridge under arbitrary dynamic environments.

Results of this study yield measurements of the equivalent linear modal properties (frequencies, mode shapes and non-proportional damping) as well as quantitative measures of the extent and nature of nonlinear interaction forces arising from strong ground shaking. It is shown that, for the particular subset of observations used in the identification procedure, the apparent nonlinearities in the system restoring forces are quite significant, and they contribute substantially to the improved fidelity of the model. Also shown is the potential of the identification technique under discussion to detect slight changes in the structure's influence coefficients, which may be indicators of damage and degradation in the structure being monitored. Difficulties associated with accurately estimating damping for lightly damped long-span structures from their earthquake response are discussed. The technical issues raised in this paper indicate the need for added spatial resolution in sensor instrumentation to obtain identified mathematical models of structural systems with the broadest range of validity

System Identification of the Vincent Thomas Suspension Bridge using Earthquake Records

1 INTRODUCTION

1.1 Motivation and Technical Challenges

While ambient vibration testing offers advantages to system identification approaches of long time-history recording and relative stationarity in the response, analysis of the earthquake response of a complex multi-input/multi-ouput (MIMO) system allows one to get a glimpse of its critical response characteristics to strong input excitation. The system identification and damage detection of long-span structures has been an area of considerable interest due to the critical role such structures often play in civil infrastructure systems. Because of their inherent length, such structures must be viewed as having multiple inputs at the base during strong-ground motions.

A considerable amount of system identification and damage detection work has been performed on structures subjected to ambient excitations and earthquake excitations. For the most part these have been performed on relatively small highway overpass bridges, and multi-story buildings. This paper attempts to tackle the system identification problem for a long-span structure excited by multiple inputs during strong earthquake events. This problem poses challenges of performing system identification where the vibration response has a substantial nonlinear component, where the structure has multiple input excitations, and with measurements from a sensor array with low spatial resolution. These are very practical problems that demand increased attention from the civil engineering research community.

The development of reduced-order mathematical models for dispersed civil infrastructure components is essential for structural control applications as well as for global structural health monitoring methodologies based on vibration signal analysis. While there has been a considerable amount of system identification studies concerned with building-like structures under ambient, earthquake and wind excitations, as well as studies of small highway overpass bridges under such excitations, relatively few studies are available concerning long-span bridges. Although not an exhaustive list, notable studies of ambient vibration response analysis of long-span bridges include: Abdel-Ghaffar and Housner (1977), Abdel-Ghaffar and Scanlan (1985a, 1985b), Abdel-Ghaffar *et al.* (1995), Niazy, (1991), Fujino *et al.* (2000), Jones and Spartz (1990), Jones *et al.* (1992), Brownjohn *et al.* (1889, 1992), Chang *et al.* (2001), Cunha *et al.* (2001), etc.

Typically, ambient vibration studies can be conducted using very long records (sometimes hours long), which considerably assists averaging aspects of the parameter identification problem in obtaining an accu-

rate mathematical model of the structural dynamics. In addition, in contrast to the rather short duration earthquake excitation case, the ambient excitation is generally a relatively stationary process, and hence, the same structural modes are always likely to be excited to the same degree over the duration of a recording. This too, as well as the relatively low-level excitation typical of ambient monitoring is particularly advantageous in obtaining a relatively well behaved linear model of long-span bridges.

As mentioned, considerable work has been done on the analysis of buildings, highway overpass structures and other multi-span bridges subjected to strong ground motions. One of the early studies was by Beck and Jennings (1980) in which a multi-story building (one of the few instrumented at the time) subjected to the 1971 San Fernando earthquake was analyzed using linear structural identification approaches. In Werner *et al.* (1987) a highway overpass bridge was analyzed on the basis of its response to the 1979 Imperial Valley earthquake. More recent work includes that of Desroches and Fenves (1997) in which a curved California highway interchange structure was modeled based on its response to the 1992 Landers and Big Bear earthquakes. In that study, primarily linear model identification was conducted, but a few nonlinear elements were considered. Along similar lines, but using a different identification algorithm, Chaudhary *et al.* (2000) performed system identification of a base-isolated multi-span bridge in Japan subjected to the 1995 Kobe earthquake and several aftershocks. Most recently, Loh (2000) performed some preliminary analysis of a multi-span bridge in Taiwan subjected to the 1999 Chi-Chi earthquake. This analysis was performed using several identification techniques.

Even among the available publications of long-span cable-supported (suspension or stayed) bridges, there is a paucity of studies that treat the dynamic response under strong ground motion of such inherently nonlinear distributed-parameter systems as multi-input/multi-output dynamic system (Smyth *et al.* (2000b), Betti *et al.* (1993), Niazy, (1991)). These studies considered the Vincent Thomas Bridge (the subject of this paper), and clearly recognized the importance on the multi-input aspect of the bridge response to earthquake excitation. The overall lack of studies on earthquake excited long-span bridges is due not only to the added complexity of the associated analysis, but also to the limited number of adequate sensor measurements with sufficient spatial resolution to afford a meaningful processing of the data.

The damping characteristics of a long-span bridge are among the essential parameters needed for design and analysis, but which cannot be obtained from engineering drawings. In the case of the Vincent Thomas Bridge (VTB), damping estimates were required to establish the level of retrofitting required for a recent seismic upgrading project. Information from a preliminary ambient analysis of the VTB in the Abdel-Ghaffar *et al.* (1995) study (to which the authors contributed) was used to assess planned earthquake mitigation measures which have recently been completed. It is however important to note that the damping estimates obtained from ambient (or other low level) excitation tests may not reflect the inherent damping estimated from critical events such as earthquakes. This is an additional distinguishing aspect of system identification with strong motion data.

One additional feature of this study is that in the equivalent-linear modeling of the structural system, the damping estimates are not constrained to be of the classical mode type. Therefore the approach yields the optimum general viscous damping representation which is more appropriate for the control as well as the monitoring aspects of structural control applications.

1.2 Scope

With the above discussion in mind, the authors have developed an efficient identification algorithm for handling general structural systems which may or may not exhibit nonlinearity in their response. Section 2 gives an overview of the Vincent Thomas Bridge monitoring system. Section 3 presents the formulation of the identification technique to be used in this study, with a particular emphasis on identifying an equivalent linear system model based on earthquake excitation and structural response data. In Section 4, the results of the linear identification and analysis are presented, while in Section 5 a brief overview of nonlinear identification results is given. Finally, in Section 6 a discussion of the significance as well as limitations of the results is presented.

2 VINCENT THOMAS BRIDGE AND ITS DYNAMIC MONITORING SYSTEM

2.1 Vincent Thomas Bridge and Sensor Array

The Vincent Thomas Bridge is located in San Pedro, California, and is a major transportation artery connecting Los Angeles with its harbor. It is a cable-suspension bridge, approximately 1850 m long, consisting of a main span of approximately 457 m, two suspended side spans of 154 m each, and a ten-span approach of approximately 545m length on either end. The roadway accommodates four lanes of traffic. The bridge was completed in 1964, and in 1980 was instrumented with twenty-six accelerometers as part of a seismic upgrading project. Currently, the sensor network is maintained by the California Division of Mines and Geology (CDMG) through the California Strong Motion Instrumentation Program (CSMIP).

Figure 1 shows the layout of the location of all the 26 sensors mounted on the bridge. A summary of the sensor numbering system and measurement directions is presented in Table 1. Notice that the eastern half of the bridge is more densely instrumented. This is because the analog recorder is housed in the eastern cable anchorage. Sixteen accelerometers are distributed at various locations and in lateral, longitudinal and vertical directions about the superstructure itself. Note that the sensor at Station 22 produced bad data and its measurement will be ommitted in the following analysis. Ten accelerometers measure motion at the substructure footings. Because the accelerometers were placed at locations on the footings of the substructure, the effects of soil-structure interaction need not be considered in the system identification

Category of Sensor and Station No.	Sensor Location	Sensor Direction w.r.t. Bridge
22,15,16,17,18,21	truss top, i.e., deck	vertical
2,4,5,6,7	truss top, i.e., deck	lateral
12	truss top, i.e., deck	longitudinal
3	truss bottom	lateral
8	tower	lateral
10,11	tower	longitudinal
14,19,20	tower base	vertical
1,9	tower base	lateral
13,23	tower base	longitudinal
26	anchorage	vertical
24	anchorage	lateral
25	anchorage	longitudinal

Table 1: Vincent Thomas Bridge sensor locations. (Note that channel 22 contains bad data.)

process. These measurements may be viewed as direct inputs into the structure, because they already include the effects of the soil-structure interaction. This differs from the often-encountered scenario, where nearby free-field recordings are considered to be excitation input, and where soil-structure interaction effects must be considered in the structural identification process.

2.2 Earthquake Response Data Sets

Since its installation, the instrumentation network has been automatically triggered twice during large seismic events in southern California. The first was for the 1987 Whittier-Narrows earthquake (M = 6.1), and the second was for the 1994 Northridge earthquake (M = 6.7). The proximity of these earthquake epicenters relative to the Vincent Thomas Bridge is shown in Fig. 2. Despite the greater distance to Northridge, because of the larger magnitude of that earthquake, the observed peak input and response accelerations ranged anywhere from 1.5 to 3 times of those recorded during the Whittier-Narrows earthquake.

For both Whittier and Northridge earthquake records, the instrument and baseline-corrected acceleration, velocity and displacement were processed by CSMIP and adopted in this study. The recorded time lengths were 80 and 120 seconds, respectively. Accordingly, the fully processed data lengths were 4000 and 6000 points, respectively. During the Northridge earthquake, Station/Channel 22 did not start at the beginning of the record. Therefore, the measurement from this station was excluded from this study. Typical ground motion and structural response records from both earthquakes are plotted in Fig. 3. It can be seen that both the excitation and response are highly non-stationary processes.

3 FORMULATION OF TIME-DOMAIN IDENTIFICATION APPROACH

The system identification procedure used in this study consists of two basic stages. The first is to identify a reduced-order linear model, and the second is to treat the unmodeled response not simply as error, but rather as unmodeled linear dynamics as well as nonlinear dynamics still to be modeled. The first step involves the identification of an equivalent linear reduced-order model of the structural system. The methodology was first presented in Masri *et al.* (1987a,b), and is summarized in the following section.

3.1 Overview of time-domain identification approach

The complex structural system is treated as a reduced-order discrete dynamic system subjected to ground excitation at discrete locations. The symbol n_1 represents the system degrees-of-freedom and n_0 the number of base (or support) excitations. The equation of motion for such a system is given in Eq. (1), and is pre-multiplied by $\mathbf{M}_{11}^{-1}$. The $\mathbf{M}_{11}$, $\mathbf{C}_{11}$ and $\mathbf{K}_{11}$ matrices have the same meaning as the more typical M, C, K notation of the mass, damping and stiffness matrices.

$$\mathbf{M}_{11}^{-1}\mathbf{C}_{11}\dot{\mathbf{x}}_1(t) + \mathbf{M}_{11}^{-1}\mathbf{K}_{11}\mathbf{x}_1(t) + \mathbf{M}_{11}^{-1}\mathbf{M}_{10}\ddot{\mathbf{x}}_0(t) + \mathbf{M}_{11}^{-1}\mathbf{C}_{10}\dot{\mathbf{x}}_0(t) + \mathbf{M}_{11}^{-1}\mathbf{K}_{10}\mathbf{x}_0(t) = -\mathbf{I}\ddot{\mathbf{x}}_0(t) \quad (1)$$

where

$$\begin{aligned}\mathbf{x}_1(t) &= [x_{11}(t), ..., x_{1n_1}(t)]^T \\ \dot{\mathbf{x}}_1(t) &= [\dot{x}_{11}(t), ..., \dot{x}_{1n_1}(t)]^T \\ \ddot{\mathbf{x}}_1(t) &= [\ddot{x}_{11}(t), ..., \ddot{x}_{1n_1}(t)]^T\end{aligned}$$

represent the measured response ("active") displacement, velocity and acceleration, respectively, and

$$\begin{aligned}\mathbf{x}_0(t) &= [x_{01}(t), ..., x_{0n_0}(t)]^T \\ \dot{\mathbf{x}}_0(t) &= [\dot{x}_{01}(t), ..., \dot{x}_{0n_0}(t)]^T \\ \ddot{\mathbf{x}}_0(t) &= [\ddot{x}_{01}(t), ..., \ddot{x}_{0n_0}(t)]^T\end{aligned}$$

represent the measured ground displacement, velocity and acceleration, respectively. The system matrices and their shorthand notations and dimensions are as follows:

Matrix product	$\mathbf{M}_{11}^{-1}\mathbf{C}_{11}$	$\mathbf{M}_{11}^{-1}\mathbf{K}_{11}$	$\mathbf{M}_{11}^{-1}\mathbf{M}_{10}$	$\mathbf{M}_{11}^{-1}\mathbf{C}_{10}$	$\mathbf{M}_{11}^{-1}\mathbf{K}_{10}$
Shorthand notation	${}^{2}\mathbf{A}$	${}^{3}\mathbf{A}$	${}^{4}\mathbf{A}$	${}^{5}\mathbf{A}$	${}^{6}\mathbf{A}$
Dimension	$(n_1 \times n_1)$	$(n_1 \times n_1)$	$(n_1 \times n_0)$	$(n_1 \times n_0)$	$(n_1 \times n_0)$

Table 2: Shorthand notation for the identified system matrices.

Equation (1), contains n_1 number of parallel equations corresponding to each degree-of-freedom and holds true at any time instance. Applying Eq. (1) to discrete time-steps, $t = \begin{bmatrix} t_1, & ..., t_N \end{bmatrix}$, where N is the

time step index, yields parallel matrix equations as follows:

$$\begin{gathered}\mathbf{M}_{11}^{-1}\mathbf{C}_{11}\dot{\mathbf{x}}_1(t_1)+\mathbf{M}_{11}^{-1}\mathbf{K}_{11}\mathbf{x}_1(t_1)+\mathbf{M}_{11}^{-1}\mathbf{M}_{10}\ddot{\mathbf{x}}_0(t_1)+\mathbf{M}_{11}^{-1}\mathbf{C}_{10}\dot{\mathbf{x}}_0(t_1)+\mathbf{M}_{11}^{-1}\mathbf{K}_{10}\mathbf{x}_0(t_1)=-\mathbf{I}\ddot{\mathbf{x}}_1(t_1)\\ \vdots\\ \mathbf{M}_{11}^{-1}\mathbf{C}_{11}\dot{\mathbf{x}}_1(t_N)+\mathbf{M}_{11}^{-1}\mathbf{K}_{11}\mathbf{x}_1(t_N)+\mathbf{M}_{11}^{-1}\mathbf{M}_{10}\ddot{\mathbf{x}}_0(t_N)+\mathbf{M}_{11}^{-1}\mathbf{C}_{10}\dot{\mathbf{x}}_0(t_N)+\mathbf{M}_{11}^{-1}\mathbf{K}_{10}\mathbf{x}_0(t_N)=-\mathbf{I}\ddot{\mathbf{x}}_1(t_N)\end{gathered} \tag{2}$$

For system identification problems, one assumes that the components in the mass, damping and stiffness matrices (i.e., the above ${}^j\mathbf{A}$ matrices in Table 2, where $j=2,3,4,5,6$) are the unknowns. Realizing this, one can then group the terms appearing in Eq. (2) so as to solve the unknown system parameters. In general, Eq. (2) can be converted into the following generic format:

$$\hat{\mathbf{R}}\hat{\boldsymbol{\alpha}}=\hat{\mathbf{b}}\Leftrightarrow\begin{bmatrix}\mathbf{R}&\mathbf{0}&\cdots&\mathbf{0}\\ \mathbf{0}&\mathbf{R}&&\\ \vdots&&\ddots&\\ \mathbf{0}&&&\mathbf{R}\end{bmatrix}\begin{bmatrix}\boldsymbol{\alpha}_1\\ \boldsymbol{\alpha}_2\\ \vdots\\ \boldsymbol{\alpha}_{n_1}\end{bmatrix}=\begin{bmatrix}\mathbf{b}_1\\ \vdots\\ \mathbf{b}_i\\ \vdots\\ \mathbf{b}_{n_1}\end{bmatrix} \tag{3}$$

where $\hat{\boldsymbol{\alpha}}$ contains all the unknown parameters to be identified, $\hat{\mathbf{R}}$ is equivalent to a coefficient matrix assembled from data measurements, and $\hat{\mathbf{b}}$ is the re-organized RHS of Eq. (2).

Equation (3) may be formulated in several ways depending upon the assumptions which are made or by using *a priori* knowledge of certain parameters in the system matrices (Masri *et al.*, 1987). Eq. (3) shows the case when no symmetric condition is assumed for the system matrices ($\mathbf{M}_{11}$, $\mathbf{C}_{11}$ and $\mathbf{K}_{11}$) to be identified. There is a total of $(2n_1+3n_0)\times n_1$ number of unknowns in the ${}^j\mathbf{A}$ matrices ($j=2,3,4,5,6$) and they are imbedded in $\hat{\boldsymbol{\alpha}}$ which has a dimension of $(n_1\,(2n_1+3n_0)\times 1)$. In Eq. (3),

$$\boldsymbol{\alpha}_i=\begin{bmatrix}{}^2(\boldsymbol{\alpha}_i) & {}^3(\boldsymbol{\alpha}_i) & {}^4(\boldsymbol{\alpha}_i) & {}^5(\boldsymbol{\alpha}_i) & {}^6(\boldsymbol{\alpha}_i)\end{bmatrix}^T \tag{4}$$

and ${}^j(\boldsymbol{\alpha}_i)$ is the ith row of ${}^j\mathbf{A}$ matrix ($j=2,3,4,5,6$). Also, $\hat{\mathbf{b}}$ has a dimension of $(n_1N\times 1)$, and

$$\mathbf{b}_i=\begin{bmatrix}-\ddot{x}_{1i}(t_1) & -\ddot{x}_{1i}(t_2) & -\ddot{x}_{1i}(t_3) & \cdots & -\ddot{x}_{1i}(t_N)\end{bmatrix}^T,\qquad i=1,...,n_1 \tag{5}$$

The matrix $\mathbf{R}$ has a dimension of $N\times(2n_1+3n_0)$ and is composed of measured data. Note that because there are n_1 identical $\mathbf{R}$'s, the $\boldsymbol{\alpha}_i$'s can then be solved directly from:

$$\mathbf{R}\boldsymbol{\alpha}_i=\mathbf{b}_i,\qquad i=1,...,n_1 \tag{6}$$

That is, each row of the ${}^j\mathbf{A}$ matrices is identified independently. Note that in general ${}^j\mathbf{A}$ will be unsymmetric even when $\mathbf{M}_{11}$, $\mathbf{C}_{11}$ and $\mathbf{K}_{11}$ are symmetric.

For each i value in Eq. (6), the number of equations, N, is normally much greater than the total number of unknowns, $(2n_1+3n_0)$. Consequently, the parameters of the matrix clusters shown above are obtained by

posing the problem as a series of overdetermined equations and then determining the unknown parameters by least-squares methods, i.e., by obtaining the pseudoinverse of the $\mathbf{R}$ matrix. This can be written as follows:

$$\hat{\boldsymbol{\alpha}} = \hat{\mathbf{R}}^{\dagger}\hat{\mathbf{b}} \qquad \text{or} \qquad \boldsymbol{\alpha}_i = \mathbf{R}^{\dagger}\mathbf{b}_i \tag{7}$$

where † stands for the pseudoinverse of a matrix.

It should be noted that in cases of force excited structures, rather than base excitation (as is the case with earthquakes), that an additional constraint of symmetry in the $\mathbf{M}_{11}$, $\mathbf{C}_{11}$ and $\mathbf{K}_{11}$ matrices can be imposed on the least-squares solution; this was done in Smyth *et al.* (2000a).

3.2 Identification of nonlinear residual terms

Once the unknown linear system matrix coefficients have been determined they may be inserted into Eq. (3) to yield an estimated $\mathbf{b}$ vector, denoted as $\mathbf{b}^{est}$, which simply contains estimates of the accelerations of the active degrees of freedom. Rather than treating the difference $(\mathbf{b} - \mathbf{b}^{est})$ as modeling error, one can treat it as a nonlinear residual, $\mathbf{b}_{nl}$, to be modeled. There are several nonlinear modeling techniques available to us, however a nonparametric technique was chosen here. Each residual in acceleration was fitted by forming a set of basis functions from the measured displacements and velocities of the active degrees of freedom and the accelerations of the base (Smyth, 1998). These basis functions were generated by producing all possible 3rd order power combinations of all of these signals. These were then arranged just as in Eq. (3) (where only 1st order, i.e., linear model, basis functions were assumed) and a new set of unknown coefficients was identified.

3.3 Identification of modal frequencies, damping coefficients and mode shapes

The identified matrices $\mathbf{M}_{11}^{-1}\mathbf{C}_{11}$ and $\mathbf{M}_{11}^{-1}\mathbf{K}_{11}$ are not convenient for direct use if matrix $\mathbf{M}_{11}$ is not known, and this happens to be true in most practical applications of base excited structures. However, modal frequencies, modal damping coefficients and mode shapes can be derived from the above identified matrices. These three quantities give important information on the system's dynamics and they can be derived from the following standard eigenvalue problem (for example, Inman 1994):

$$\mathbf{A}\mathbf{z} = \lambda\mathbf{z} \tag{8}$$

where

$$\mathbf{A} = \begin{bmatrix} \mathbf{0} & \mathbf{I} \\ -\mathbf{M}_{11}^{-1}\mathbf{K}_{11} & -\mathbf{M}_{11}^{-1}\mathbf{C}_{11} \end{bmatrix} \tag{9}$$

Since $\mathbf{M}_{11}^{-1}\mathbf{K}_{11}$ and $\mathbf{M}_{11}^{-1}\mathbf{C}_{11}$ are identified by the above, the matrix $\mathbf{A}$ is thus identified. It has a dimension of $2n_1$ by $2n_1$. The eigenvalue λ_k $(k = 1, 2, \ldots, 2n_1)$ of $2n_1$ numbers may be complex valued.

If so, the eigenvector $\mathbf{z}_k$ ($k = 1, 2, \ldots, 2n_1$) of $2n_1$ numbers, with a dimension of $2n_1$ each, may be complex valued.

The complex eigenvalues λ_k ($k = 1, 2, \ldots, 2n_1$) come in complex conjugate pairs. The n_1 physical modal frequencies, ω_i, and modal damping coefficients, ζ_i, are related to λ_k by:

$$\omega_i = \sqrt{\mathrm{Re}(\lambda_{2i-1})^2 + \mathrm{Im}(\lambda_{2i-1})^2} = \sqrt{\mathrm{Re}(\lambda_{2i})^2 + \mathrm{Im}(\lambda_{2i})^2}, \qquad i = 1, ..., n_1 \tag{10}$$

$$\zeta_i = \frac{-\mathrm{Re}\left(\lambda_{2i-1}\right)}{\sqrt{\mathrm{Re}\left(\lambda_{2i-1}\right)^2 + \mathrm{Im}\left(\lambda_{2i-1}\right)^2}} = \frac{-\mathrm{Re}\left(\lambda_{2i}\right)}{\sqrt{\mathrm{Re}\left(\lambda_{2i}\right)^2 + \mathrm{Im}\left(\lambda_{2i}\right)^2}}, \qquad i = 1, ..., n_1 \tag{11}$$

where $\mathrm{Re}(\cdot)$ means the real part of a complex number, and $\mathrm{Im}(\cdot)$ the imaginary part.

The $2n_1$ dimension complex eigenvectors $\mathbf{z}_k$ ($k = 1, 2, ..., 2n_1$) of $2n_1$ numbers also come in complex conjugate pairs. They are related to the n_1 dimension complex mode shapes $\mathbf{u}_i = \mathbf{a}_i + \mathbf{b}_i j$ ($i = 1, \ldots, n_1, j = \sqrt{-1}$) in the following manner:

$$\begin{aligned} \mathbf{z}_{2i-1} &= \begin{bmatrix} \mathbf{u}_i \\ \lambda_{2i-1}\mathbf{u}_i \end{bmatrix}, \qquad i = 1, ..., n_1 \\ \mathbf{z}_{2i} &= \begin{bmatrix} conj(\mathbf{u}_i) \\ \lambda_{2i} conj(\mathbf{u}_i) \end{bmatrix}, \qquad i = 1, ..., n_1 \end{aligned} \tag{12}$$

It can be seen that the first n_1 rows of the eigenvectors with odd subscript, i.e., $\mathbf{z}_{2i-1}$, form the n_1 dimension complex mode shapes $\mathbf{u}_i$ ($i = 1, \ldots, n_1$). Thus, it has been shown how the complex modal frequencies, damping coefficients and complex mode shapes are derived from the identified $\mathbf{M}_{11}^{-1}\mathbf{C}_{11}$ and $\mathbf{M}_{11}^{-1}\mathbf{K}_{11}$ matrices. Details are shown in Appendix B.

4 LINEAR IDENTIFICATION RESULTS

For this problem, the continuous structural system of the Vincent Thomas Bridge is analyzed as a reduced-order discrete system based on the 15 structural response locations and 10 support inputs. The parameter values of $n_1 = 15$ and $n_0 = 10$ are substituted into the above formulae. Because this represents a *reduced-order* model of what is likely to be a more complex system with more degrees-of-freedom and support motions, the modeling of this system using Eq. (1) will naturally incorporate some error due to these unavailable measurements. This inherent limitation, due to low spatial resolution of the sensing, affects the range of conclusions which can be drawn from the identified reduced-order model.

4.1 Shifted window identification for nonstationary process analysis

It is not surprising that, given the highly nonstationary nature of earthquake ground motions, the measurements of base and structural accelerations were also highly nonstationary for both earthquake events as shown in Fig. (3). From preliminary analysis, it was also suspected that during the time of strongest shaking, the response had a significant nonlinear component. This may have been due to several factors including geometric nonlinearities caused by large deformations, and/or perhaps "rattling" of expansion joints in the bridge deck. From visual inspection of acceleration time history data in Fig. (4) from channels 6, 12 and 2 which are all located at or near tower-to-deck connections, one can see periodic impulses. This is undoubtedly as a result of banging and slipping of the "wind shoe" which provides the deck with vertical and transverse support at the tower-to-deck connections. In fact there is physical evidence to support this: only a few weeks before the Northridge earthquake the bridge was painted in the area of the "wind shoes", and after the earthquake, clear signs of scraped paint were observed, indicating substantial deck movement relative to the tower (Abdel-Ghaffar, 2001).

With this in mind, one must be careful with the idea of linearization as well as interpreting the results obtained from this type of equivalent linearization technique. Identification of the residual, composed of nonlinear as well as unmodeled linear dynamics, is briefly discussed here, but is not the main focus of this study (rather it will be the focus of future research). Instead, an attempt is made to seek an equivalent linear model for the system based on the structural response during the earthquake. The equivalent linear model can be used to assess the structural integrity after the earthquake.

Because different levels of nonlinearity were suspected to occur during different periods of shaking, identification could be performed on various time windows of the recorded measurements. The identification procedure can be performed over relatively short windows and then each window can be shifted by a small amount until the end of the data set is reached. These types of results can be compiled to track structural changes during the excitation process. Statistical results from the shifted response segments can be an indication of changing structural dynamics.

Because the first part of each earthquake contained the strongest motion and was quite nonstationary, it is expected that the greatest nonlinearity in response would occur during this time. With this in mind, and because a linearization technique is being employed, some of the shifting window identification results presented in this study will be from only the second half of the response records. There is no particular rationale for choosing the suitable window length for the identification, other than to consider the tradeoff between including enough points to make an overdetermined system of equations, and still being able to capture any possible time variation. Because of this, a few window lengths were tested, and their results compared.

4.2 Identified modal frequencies and damping ratios

It is important to stress that, unlike many methods which yield only modal frequencies and damping estimates, in this paper these quantities are actually computed indirectly after the complete reduced order system matrices are identified. In fact, the identification procedure makes no assumption of classical normal modes, and thus we get information on the nonproportional damping. Unfortunately, however, because this is a base-motion input case, and not a force-excited example, it is only possible to identify the cluster of system matrices premultiplied by the inverse of the mass matrix.

For the reduced order modeling of the Vincent Thomas Bridge, the number of degrees-of-freedom is 15 (corresponding to the number of sensors at active DOF's). Therefore, 15 modal frequencies and damping ratios respectively can be identified from each time-history window.

As previously mentioned, the identification procedure is performed over relatively narrow windows. The window lengths which were used are 1000 and 2000 continuous measurement points (i.e, about 4.2, and 8.4 fundamental periods) for the Whittier earthquake and 1000, 2000 and 3000 points (i.e, about 4.2, 8.4 and 12.6 fundamental periods) for the Northridge earthquake, respectively. The short windows are shifted with 10 points overlap with their previous window in all the cases. The shifting windows start from the very beginning of the time period under consideration and end when the end of the data-set is reached. As mentioned earlier, because this is a base excited case, the identification procedure was performed without invoking any symmetry assumption in matrices $\mathbf{M}_{11}$, $\mathbf{C}_{11}$ and $\mathbf{K}_{11}$.

Variations in identified modal frequencies and modal damping ratios using the shifted window approach from the second half of the Northridge response record, are plotted in Figures (5a) and (6a) relative to the window length used. In these figures the variation is shown by giving the mean, maximum and minimum values obtained for the set of shifted windows. It is not surprising that the dispersion is greater for the shorter window length. The shorter window also places more importance on high frequency modes, by identifying slightly higher frequencies for the highest modes. In addition, the second column (b) in each of these figures shows the same results for identification analysis performed using the entire record length. The mean values of the identified frequencies are quite similar, except for the fact that higher frequencies are again identified for the highest modes. Not surprisingly also, because the nonstationary and presumably nonlinear response portion of the time-history is now included, the distribution range from minimum to maximum is noticeably larger for both the identified frequencies and damping ratios.

Using the type of mode-number frequency and damping statistics just presented should be done with great care. This is because the total number of modes which can be determined by this method is in essence fixed to be the same as the number of active degrees of freedom (n_1), and therefore it is quite possible that for a system which is in reality of a higher order, that the technique under discussion will identify n_1 modes which are not the same as the n_1 modes in the next time window. In other words, the least-squares

based approach will identify the n_1 order system which yields the dominant motion for that particular response time interval. This can be considered a limitation or a strength of the method, depending upon the application. This feature is common to all methods which seek to obtain a 2nd order model (as in Eq. (1)) with physically meaningful coordinates based on discrete location measurements, with no additional *a priori* information on the system dynamics.

Because one cannot draw conclusions from the variation over time of a given mode-number, one is left with possibly tracking a particular mode by its mode shape from data set to data set (or window to window), and comparing its frequencies and damping ratios. This will be discussed in the next section.

It is important to note also that negative damping coefficients are identified intermittently during the entire response process. This might be related to the varying magnitude and severity of the earthquake excitation process causing the response to exhibit varying levels of nonlinearity. One can see however that most of the mean values of the damping ratios are non-negative. Because the identification is relatively unconstrained, and because the equivalent linear modeling is being performed on what is suspected to be nonlinear response dynamics, there is nothing to prevent the identification of negative damping coefficients.

4.3 Identified complex mode shapes and their physical interpretations

Normally, mode shapes are used as a time-invariant basis for the displacement profile of a linear system. For a system with n_1 degrees-of-freedom, the absolute displacement x (as a function of time t) can be expressed as:

$$\mathbf{x}(t) = \sum_{i=1}^{n_1} c_i(t)\mathbf{u}_i e^{\left(-\zeta_i\omega_i - \omega_i\sqrt{1-\zeta_i^2}\,j\right)t} \tag{13}$$

where c_i's are mode shape coefficients, $\mathbf{u}_i$'s mode shapes, ζ_i's modal damping coefficients and ω_i's modal frequencies. Note here, that the $\mathbf{u}_i$'s are complex mode shapes in general.

In this study, the complex response of a nonlinear system is reduced to an equivalent linear process, and its complex mode shapes are derived. The derived mode shapes then reflect the underlying time invariant linear basis for the time window considered. However, care must be exercised with respect to how these mode shapes are related back to the complete original response. Furthermore, complex, rather than real mode shapes should be interpreted for a real structure.

In general, the mode shapes as derived in Section 3.3 are complex vectors of dimension n_1 for each mode. For any time window selected, a set of mode shape vectors can be obtained. They represent the displacement profile at $n_1 = 15$ stations for a total of $n_1 = 15$ modes. Figures (7) and (8) show the n_1=15 plots of the magnitude and phase of a representative set of the 15 mode shapes corresponding to a specific time window. Each plot is composed of $n_1 = 15$ discrete points showing the relative movements at the 15 sensor locations. In this study, all the acceleration measurements have the same units of translational

movement. For convenience, each mode shape vector is normalized to have a Euclidian norm of one. The mode-shape phase angle plots in Fig. (8) have a range of $[-\pi, \pi]$. The plots of phase angle shown in Fig. (8) are important in that they indicate which motions are coupled with one another. This information helps in understanding the interactions of major bridge components during strong earthquake responses.

To get a better feel for the deformed shape that these complex mode shapes represent, a "snap shot" is taken to project complex vectors into real vectors. To preserve features of both magnitude and phase angle, the location of the projected real and imaginary axes should be chosen to minimize the total projection onto the imaginary axis. In this case a weighted least squares methods was used to obtain the optimal reference axes. The first and fifteenth modes are plotted for major station locations and shown in Figs. (9) and (10) respectively. This 3-dimensional representation approximates the mode shapes at points between the sensor locations by straight lines. It should be noted that in order to construct these figures some assumptions were made at a few locations where sensor information was not available. For example, because the tower supports the deck truss vertically through a truss link, it was assumed that there was no vertical deflection at that deck section. Also, because the side-span vertical Station 22 was not included in the study due to a data recording problem, its vertical motion is shown based on judgement of the overall mode shape and the vertical motion of Station 21 at the other side of the roadway.

4.4 Identified results of ${}^3\mathbf{A}$ matrix

The identification of the stiffness matrix $\mathbf{K}_{11}$ enables a direct evaluation of structural integrity of the bridge, however, only $\mathbf{M}_{11}^{-1}\mathbf{K}_{11}$, i.e., the ${}^3\mathbf{A}$ matrix, can be obtained from the present identified results. 3-D bar charts of the samples of symmetrically identified ${}^3\mathbf{A}$ matrices using a 2000 points window for Whittier and Northridge earthquakes are presented in Figs. (11) and (12), respectively. The height of each bar simply represents the magnitude of each matrix coefficient, and the view from above (panel (a) of each figure) clearly shows the positive values, and the view from below (panel (b) of each figure), the negative values. It can be seen that these ${}^3\mathbf{A}$ matrices are quite unsymmetric. The diagonal terms range in magnitude from about 2-60 $(rad/sec)^2$, whereas, several off-diagonal terms, particularly in the columns corresponding to stations 3 and 4, have coefficients with magnitudes up to about 100 $(rad/sec)^2$. To further examine the variation over time in the system dynamics, histogram plots of the dominant elements of the above identified ${}^3\mathbf{A}$ matrices are shown in Figs. (13) and (14) for Whittier and Northridge earthquakes, respectively. Note that these histogram plots are all to the same scale. Clearly some terms, for example diagonal number 10 in Fig. (13), are relatively unchanged regardless of which time-window is used for the identification. This contrasts with others such as ${}^3\mathbf{A}(21, 4)$ which has considerable dispersion, indicating either variability over the duration of the total identification time-window, or an increased level of uncertainty (for any number of reasons) in identifying this parameter. The reader will observe that the values of 2-60 $(rad/sec)^2$ for the $\mathbf{M}_{11}^{-1}\mathbf{K}_{11}$ diagonal coefficients (which are in ω^2 units) correspond with the obtained modal frequencies of

about 0.2Hz-1.2Hz.

If one assumes the mass distribution does not vary, the histograms reflect variation in the stiffness matrix. These types of results can be compiled to track structural changes during the excitation process. However, this indicator of structural change is indirect. It is difficult to quantify structural alteration based only on changes in the ${}^3\mathbf{A}$ matrix without knowledge of the mass matrix or the nature (bandedness) of the stiffness matrix.

4.5 Comparison of identified results of the 1987 Whittier and 1994 Northridge earthquakes

The identification results of the structural dynamic parameters from the Whittier and Northridge earthquakes can be compared. Typically, such a comparison would entail the comparison of identified modal frequencies and damping coefficients. As previously mentioned, this must be done with some care, because what might be mode k in one case (i.e., for a selected time window) may not be mode k in another. Having said this, certain gross conclusions can perhaps be drawn from an overall comparison by mode-number. The obtained modal frequencies and damping ratios are shown in Fig. (15). Clearly there is an overall drop in modal frequencies from the Whittier earthquake to the Northridge earthquake. This can also be seen from the comparison of the histograms of the obtained diagonal coefficients of the ${}^3\mathbf{A}$ matrices. In principle, these coefficients can be compared with one another as they are directly obtained from the identification procedure and relate to each DOF. The mean values of the histogram plots of the identified diagonal elements of the ${}^3\mathbf{A}$ matrices from both earthquakes are shown in Fig. (16). There is a clear trend of reduction in the magnitude of the diagonal elements in ${}^3\mathbf{A}$ matrices from Whittier to Northridge earthquakes. From this information one can conclude (under some questionable assumptions on the bandedness and nature of the mass matrix) that there is an overall reduction of the effective stiffness of the bridge under the Northridge earthquake compared to its behavior under the Whittier one. On a cautionary note, it is important to recall that, because these matrix coefficients are obtained from an equivalent linearization procedure, and because the magnitude of the excitation was larger in the Northridge case, that some of the observed changes in identified coefficients could be due to the fact that one is in a different nonlinear response range, and not the effect of an inherent structural change. An additional figure, Fig. (17), showing the mean values of the most dominant matrix coefficients, also shows a general reduction in magnitude. Again, it is difficult to draw conclusions about changes in the stiffness matrix from this indirect information.

The modal damping estimates shown in Fig. (15) from each earthquake response include a few negative values. Clearly these have no physical meaning, but are simply the result of obtaining the optimal equivalent linear model for a very lightly damped system with probable nonlinear system dynamics. Typical estimates for long-span bridge modal damping values are on the order of 1% of critical, and as shown here, most of the damping estimates are in this range. This was shown in a more general sense earlier in Fig. (6), where

the mean values of the damping estimates are positive and on the order of about 1-2%. It should be noted that depending upon which overall time span was used for the identification, different estimates of damping were obtained. Figure (15) shows the results from using the last 3000 points of both earthquake response. This latter part of the records was specifically chosen for comparison purposes with results from a study by other investigators as discussed below.

5 NONLINEAR IDENTIFICATION RESULTS

Depending upon which time window was used for equivalent linear modeling and subsequent comparison of fits, the nonlinear residual error for the entire response time-history ranged anywhere from as low as 10 percent to as high as 85 percent, with an average residual of about 50-60 percent. A sample of these fitting errors is shown in Fig. (18). Notice in Fig. (18) how the acceleration based on the linear model matches the response reasonably well (approximately 20 percent RMS residual). This is largely attributable to the fact that the vertical deck modes dominated the response signal for this station, and were relatively easy for the linear system to model.

Residual response components, which presumably included nonlinear as well as unmodeled linear dynamics and measurement noise, remain for each active degree of freedom acceleration measurement. These were fitted with the nonparametric technique outlined earlier. An example of the performance of this method is shown in Fig. (19). In this case the fitting was performed on lateral response station 7, which had a 46 percent RMS nonlinear residual to be modeled nonparametrically. The fitting of this nonlinear component was to within 55 percent RMS error. Therefore the *entire* signal was modeled to within an accuracy of about 25.3 percent RMS error (shown in the bottom panel of Fig. (19)). This is a respectable result given that the system is presumably undergoing change during the excitation, and that the identified model is assumed to be time-invariant throughout the earthquake event.

6 DISCUSSION

Some identification results shown herein confirm that this relatively simple time-domain based identification procedure can capture, in a reduced order model, the essence of the response dynamics of this highly complex structural system. The equivalent linear identification phase yields system information which includes complex mode shapes; in other words, it makes no assumptions of proportional damping. The modal frequencies obtained for the two earthquakes are similar, but indicate some system changes. Additional detailed analysis is needed to compare these identified systems under earthquake loading with previous identification work performed on the bridge under ambient loading conditions (Abdel-Ghaffar and Housner, 1977, Abdel-Ghaffar *et al.*, 1995).

6.1 Preliminary data processing

Successful application of the time-domain identification approach adopted in this study strongly relies on the accuracy of the acceleration, velocity and displacement data set. When the acceleration is the only measurement available, care must be taken when integrating acceleration data to get the corresponding velocity and displacement because this approach is known to be sensitive to the noise imbedded in the original acceleration measurement data. When the acceleration measurement is polluted with noise, the identified results can contain biases even when the signal-to-noise ratio is high. Therefore, a significant role is played by the original data quality as well as the preliminary data processing. In this study, the data used were pre-processed by California Strong Motion Instrumentation Program (CSMIP). They are the instrument and baseline-corrected acceleration, velocity and displacement.

6.2 Comparison with other identification methodologies

Other published investigations have been conducted on the Vincent Thomas Bridge, although principally based on ambient measurement data (for example, Niazy (1991), and Housner and Abdel-Ghaffar (1977)). The frequencies and mode shapes determined in this study are similar to those obtained in the aforementioned ambient studies, but show some differences, which is expected given that the bridge underwent some minor structural changes during a retrofit between the time of the ambient testing and the earthquakes considered here. In Niazy (1991), the Whittier earthquake data-set is also used for identification purposes. In Luş *et al.* (1999), the Whittier and Northridge responses of the Vincent Thomas Bridge were also considered using the Observer Kalman Filter IDentification (OKID) approach (Juang *et al.*, 1993). This time-domain, first order, discrete linear identification approach is capable of obtaining an arbitrarily high number of modes, but in states which have no physical meaning. In the Luş *et al.* study, the authors modeled five vertical deck location responses based on all ten base inputs. As previously mentioned, the vertical deck motions can clearly be seen to behave quite linearly, and were hence modelled to a high degree of accuracy with a large number of modes. In contrast, in this study the responses of all available 15 active DOF's were modeled with the fixed size reduced-order model. This is therefore a more challenging identification problem. Table 3 gives some of the results obtained for both earthquake data-sets.

In the table, several modal frequencies have been highlighted with a '$\star$' symbol for comparison with similar results in the Luş *et al.* study. These modes exhibited a significant vertical component in the mode shapes, and this explains why they were also detected by the Luş *et al.* study which concentrated only on those modes. The accuracy in agreement with the other study is very good.

The identification method employed in Luş *et al.* is constrained to give only positive damping estimates, and does not therefore yield the few negative damping estimates obtained in this study. In addition, the difficulties associated with accurate estimation of damping from this type of data-set may be seen from the

Smyth *et al.* Dominant Modes (All directions)				Luş *et al.* (1999) Vertical Comp. Modes			
Whittier		Northridge		Whittier		Northridge	
ω (Hz)	ζ	ω (Hz)	ζ	ω (Hz)	ζ	ω (Hz)	ζ
⋆ 0.212	0.012	⋆ 0.225	0.001	0.234	0.015	0.225	0.017
⋆ 0.242	0.017	⋆ 0.240	0.082	0.388	0.382	0.304	0.286
⋆ 0.317	-0.043	⋆ 0.358	-0.047	0.464	0.097	0.459	0.018
0.531	0.102	0.390	0.042	0.576	0.099	0.533	0.040
⋆ 0.570	0.006	⋆ 0.448	-0.007	0.617	0.145	0.600	0.262
0.636	0.042	⋆ 0.478	0.013	0.617	0.768	0.632	0.137
⋆ 0.672	0.001	⋆ 0.522	0.014	0.769	0.297	0.791	0.156
0.734	0.024	⋆ 0.587	-0.001	0.804	0.014	0.811	0.010
⋆ 0.818	0.019	0.625	0.074	0.857	0.116	0.974	0.027
⋆ 0.958	0.029	0.733	0.012	0.947	0.043	1.110	0.006
1.027	-0.019	0.837	0.050	–	–	–	–
⋆ 1.111	0.013	⋆ 0.935	-0.018	–	–	–	–
⋆ 1.159	0.017	1.036	0.016	–	–	–	–
1.391	0.023	1.110	0.017	–	–	–	–
1.554	-0.013	⋆ 1.136	0.014	–	–	–	–

Table 3: Identified modal frequencies and damping ratios obtained by analyzing the last 3000 points of both the Whittier and Northridge earthquake data sets. Note that the set of modes indentified for a given data set may not correspond to the identified mode numbers for another data set.

fact that very high damping estimates can also be obtained. In this study no large damping values were obtained, however, the Luş *et al.* study identified several modes with very high damping, in one case as high as 77% of critical.

7 CONCLUSION

The dominant dynamic characteristics of the Vincent Thomas Bridge response to both the 1987 Whittier and 1994 Northridge earthquakes are modeled using a combination of linear and nonlinear system identification techniques. From the equivalent linear modeling results, some structural changes are detected, although definitive conclusions are impossible to make without making assumptions. Some of the difficulties of identifying the structural dynamics of a long-span flexible bridge to nonstationary earthquake multi-input base excitation are illustrated and discussed. These difficulties include the low spatial resolution of the sensor array, and presumed time variation of the actual structure, presumed nonlinear response contribution, incomplete excitation information, and measurement noise. The range of validity of the identified reduced-order model for this type of study would be enhanced with increased spatial resolution of sensor instrumentation. It is shown that the approach of this paper is useful in obtaining the optimum (in a least-squares sense) equivalent linear properties of multi-input/multi-output structures based on a relatively short observed response

under nonstationary excitation.

8 ACKNOWLEDGMENTS

The data in this study was gathered by the California Division of Mines and Geology through the California Strong Motion Instrumentation Program. This study was supported in part by the United States Air Force Office of Scientific Research, the National Science Foundation and the Federal Emergency Management Agency. Discussions with Prof. Abdel-Ghaffar are greatly appreciated.

9 REFERENCES

Abdel-Ghaffar, A. M. and Housner, G. W.,(1977), "An analysis of the dynamic characteristics of a suspension bridge by ambient vibration measurements," *Earthquake Engineering Research Laboratory, California Institute of Technology, Report EERL*, pp 77-01.

Abdel-Ghaffar, A. M., Masri, S. F. and Nigbor, R. N., (1995), "Preliminary report on the Vincent Thomas Bridge monitoring test," *Center for Research in Earthquake and Construction Engineering*, University of Southern California, Report No. M9510.

Abdel-Ghaffar, A.M., and Scanlan, R.H., (1985a), "Ambient Vibration Studies of Golden Gate Bridge: I Suspended Structure," *ASCE Jo. of Engineering Mechanics,* Vol. 111, No. 4, pp. 463-482.

Abdel-Ghaffar, A.M., and Scanlan, R.H., (1985b), "Ambient Vibration Studies of Golden Gate Bridge: II Pier-Tower Structure," *ASCE Jo. of Engineering Mechanics,* Vol. 111, No. 4, pp. 483-499.

Abdel-Ghaffar, A.M., (2001), personal communication with Prof. Abdel-Ghaffar.

Beck, J.L., and Jennings, P.C., (1980), "Structural Identification using Linear Models and Earthquake Records," *Earthquake Engineering and Structural Dynamics,* Vol. 8, pp. 145-160.

Brownjohn, J.M.W., Dumanoglu, A.A., Severn, R.T., and Blakeborough, A., (1989), "Ambient Vibration Survey of the Bosporus Suspension Bridge," *Earthquake Engineering and Structural Dynamics,* Vol. 18, pp. 263-283.

Brownjohn, J.M.W., Dumanoglu, A.A., and Severn, R.T., (1992), "Ambient Vibration Survey of the Fatih Sultan Mehmet (Second Bosporus) Suspension Bridge," *Earthquake Engineering and Structural Dynamics,* Vol. 21, pp. 907-924.

Chang, C.C., Chang, T.Y.P., and Zhang, Q.W., (2001), "Ambient Vibration of Long-Span Cable-Stayed Bridge," *ASCE Jo. of Bridge Engineering,* Vol. 6, No. 1, January/February, pp. 46-53.

Chaudhary, T.A., Abe, M., Fujino, Y., and Yoshida, J., (2000), "System Identification of Two Base-Isolated Bridges Using Seismic Records," *ASCE Jo. of Structural Engineering,* Vol. 126, No. 10, October, pp. 1187-1195.

Cunha, A., Caetano, E., and Delgado, R., (2001), "Dynamic Tests on Large Cable-Stayed Bridge," *ASCE Jo. of Bridge Engineering,* Vol. 6, No. 1, January/February, pp. 54-62.

Desroches, R., and G.L. Fenves, (1997), "Evaluation of Recorded Earthquake Response of a Curved Highway Bridge," *Earthquake Spectra,* Vol. 13, No. 3, pp. 363-386.

Fujino, Y., Abe, M., Shibuya, H., Yanagihara, M., Sato, M., Nakamura, S.-I., Sakamoto, Y., (2000), "Forced and Ambient Vibration Tests and Vibration Monitoring of Hakucho Suspension Bridge Source," *Transportation research record,* no. 1696, pp. 57.

Inman, R. J., (1994), Engineering Vibration, Prentice Hall, pp. 560.

Jones, N. P. and Spartz, C. A., (1990), "Structural Damping Estimation for Long-Span Bridges," *Journal of Engineering Mechanics, ASCE,* 16(11), November, pp. 2414-2433.

Jones, N.P., Thompson, J.M., and Wilson, J.C., (1992), "Ambient Vibration Survey of Baytown Bridge Towers," *Proc. Structures Congress, ASCE,* April, 230-233.

Juang, J. N., Phan, M., Horta, L.G., and Longman, R.W., (1993), "Identification of observer/Kalman filter Markov parameters: theory and experiments," *J. Guidance Control Dyn.,* **16**(2), pp. 320-329.

Loh, C.-H., (2000), "Seismic Response Measurement and System Identification of Bridges," *Proc. of the 1st MCEER Workshop on Mitigation of Earthquake Disaster by Advanced Technologies (MEDAT-1),* Technical Report MCEER-00-0009, Nov. 19, Los Angeles, CA, pp. 87-105.

Luş, H., Betti, R., and Longman, R.W., (1999), "Identification of Linear Structural Systems using Earthquake-Induced Vibration Data," *Earthquake Engineering and Structural Dynamics,* **28**, pp. 1449-1467.

Masri, S. F., Miller, R. K. Saud, A. F. and Caughey, T. K., (1987a), "Identification of nonlinear vibrating structures: part I - formulation," *J. of Applied Mechanics*, 54, pp 918-929.

Masri, S. F., Miller, R. K. Saud, A. F. and Caughey, T. K., (1987b), "Identification of nonlinear vibrating structures: part II - applications," *J. of Applied Mechanics*, 54, pp 918-929.

Niazy, A. M., (1991), " Seismic performance evaluation of suspension bridges," *Ph.D. Dissertation,* University of Southern California.

Smyth, A. W., (1998), "Analytical and experimental studies in system identification and monitoring in the context of structural control," *Ph.D. Dissertation*, University of Southern California.

Smyth, A. W., Masri, S.F., Caughey, T.K., and Hunter, N.F., (2000a), "Surveillance of Mechanical Systems on the Basis of Vibration Signature Analysis," *ASME Jnl. of Applied Mechanics*, Vol. 67, September, pp. 540-551.

Smyth, A.W., Masri, S.F., Abdel-Ghaffar, A.M., and Nigbor, R.N., (2000b), "System Identification and Damage Detection of a Long-Span Suspension Bridge based on its Dynamic Response to Major Earthquake Excitations," 12th World Conference on Earthquake Engineering, Auckland, New Zealand, Oct.

Werner, S.D., Beck, J.L., Levine, M.B., (1987), "Seismic Response Evaluation of Meloland Raod Overpass using 1979 Imperial Valley Earthquake Records," *Earthquake Engineering and Structural Dynamics,* Vol. 15, pp 249-274.

List of Figures

1 Accelerometer locations and directions for the instrumentation network on the Vincent Thomas Bridge. . . . 22

2 Map showing the location of the Vincent Thomas Bridge, and its proximity to the 1987 Whittier Narrows earthquake and the 1994 Northridge earthquake. . . . 23

3 Typical ground motion and structural response time-histories for both earthquakes. . . . 24

4 A 20 second window of the measured acceleration response at stations 2, 6, and 12. These accelerograms (particularly those for stations 2 and 6) indicate impulsive accelerations, not seen in any other response records. These locations correspond to the tower-to-deck "wind shoe" connection area, and indicate a significant slipping and banging type of nonlinear behavior. . . . 25

5 Variation in maximum, minimum and mean value from (a) the second half history, and (b) the entire records, of unsymmetrically identified modal frequencies for the Northridge earthquake with different window lengths. T_1 is the fundamental period of the identified model for the bridge and was found to be about 4.5 seconds in most of the results. . . . 26

6 Variation in maximum, minimum and mean value from (a) the second half history, and (b) the entire records, of unsymmetrically identified modal damping ratios for the Northridge earthquake with different window lengths. T_1 is the fundamental period of the identified model for the bridge and was found to be about 4.5 seconds in most of the results. . . . 27

7 Magnitude plot of a normalized complex mode shapes. The example used here is of the identified mode shapes from the Northridge earthquake with a window covering the last 3000 points in the recorded history. . . . 28

8 Phase angle plot of the normalized complex mode shapes. The results shown here are from the identified mode shapes for the Northridge earthquake data with a window covering the last 3000 points in the recorded history. . . . 29

9 Snap shot of the normalized complex 1st mode. The example used here is from the Northridge earthquake data with a time window covering the last 3000 points in the recorded history. . . . 30

10 Snap shot of the normalized complex 15th mode. The example used here is from the Northridge earthquake data with a time window covering the last 3000 points in the recorded history. . . . 31

11 3-D bar chart (view from above (a) and below (b)) of the identified $^3\mathbf{A}$ matrix for the Whittier earthquake. The coefficient indices in the $^3\mathbf{A}$ matrix are related to the original station numbers. The window length used is over the last 3000 points. . . . 32

12 3-D bar chart (view from above (a) and below (b)) of the identified $^3\mathbf{A}$ matrix for the Northridge earthquake. The coefficient indices in the $^3\mathbf{A}$ matrix are related to the original station numbers. The window length used is over the last 3000 points. . . . 33

13 Histograms showing variation in the identified 10 most dominant coefficients (in an absolute sense) in the $^3\mathbf{A}$ matrix for the Whittier earthquake. The variation was produced by performing the identification at numerous shifted windows of length 2000 points over the last 3000 points of measurement time-histories. . . . 34

14 Histograms showing variation in the same dominant coefficients shown in Fig. (13) from the $^3\mathbf{A}$ matrix for the Northridge earthquake. The variation was produced by performing the identification at numerous shifted windows of length 2000 points over the last 3000 points of measurement time-histories. . . . 35

15 Comparison of modal identified frequencies and damping ratios for the last 3000 points of the time-histories from the Whittier and Northridge earthquakes. Note that care should be taken in drawing conclusions from this because the modes are compared by their number and not by their mode shape. 36

16 Comparision of the identified mean value of diagonal elements in ${}^{3}\mathbf{A}$ matrix between Whittier and Northridge earthquake. The variation was produced by performing the identification at numerous shifted windows of length 2000 points over the last 3000 point (top panel) or the full measurement time-histories (bottom panel) for both earthquakes respectively. 37

17 Comparision of the identified mean value of the 10 most dominant elements in ${}^{3}\mathbf{A}$ matrix between Whittier and Northridge earthquake. The variation was produced by performing the identification at numerous shifted windows of length 2000 points over the last 3000 points for both earthquakes. These are the mean values from Fig. (13) and Fig. (14). 38

18 Comparison of the equivalent linear time-invariant system time history fit for the vertical response at Station 15 at the bridge midspan. Note that only the last 1500 points of the 6000 sample record are shown for added resolution. Over the entire earthquake response, the fit error is approximately 20% RMS at this location. 39

19 Representative example of the nonlinear residual fitting. In the top panel, the measured station 7 (lateral, side-span) acceleration is shown. Below this is the linear, time-invariant model estimate. The middle panel shows the residual (i.e., the difference of the previous two signals). In the fourth panel the nonparametrically modeled residual is given, and finally at the bottom the remaining total error is shown. For ease of comparison, identical scales are used for all panels. 40

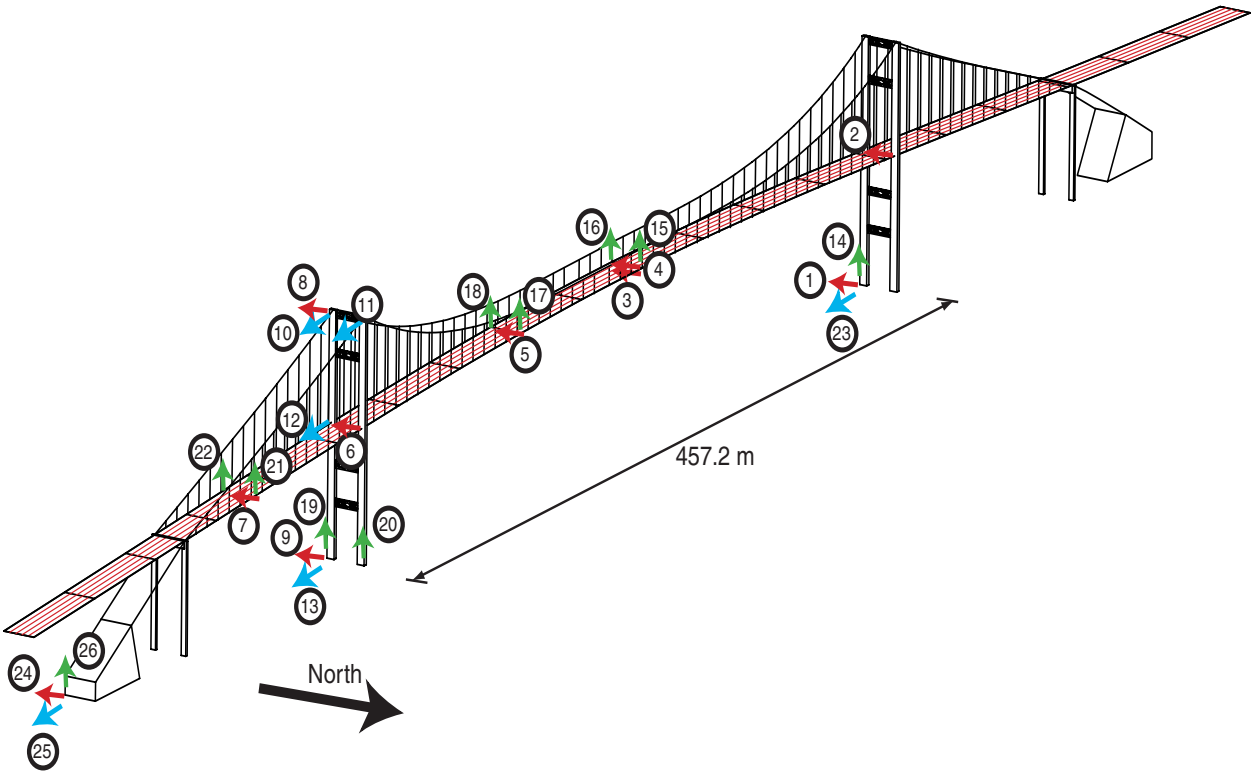

Figure 1: Accelerometer locations and directions for the instrumentation network on the Vincent Thomas Bridge.

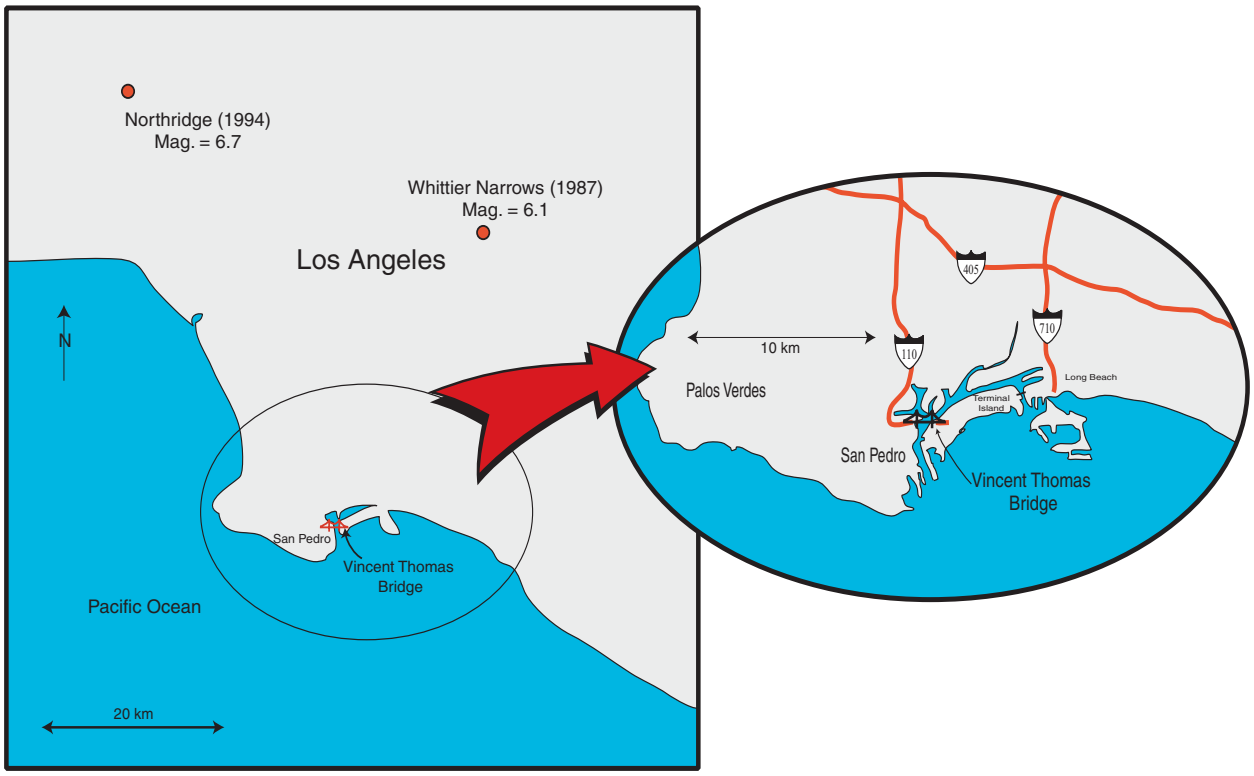

Figure 2: Map showing the location of the Vincent Thomas Bridge, and its proximity to the 1987 Whittier Narrows earthquake and the 1994 Northridge earthquake.

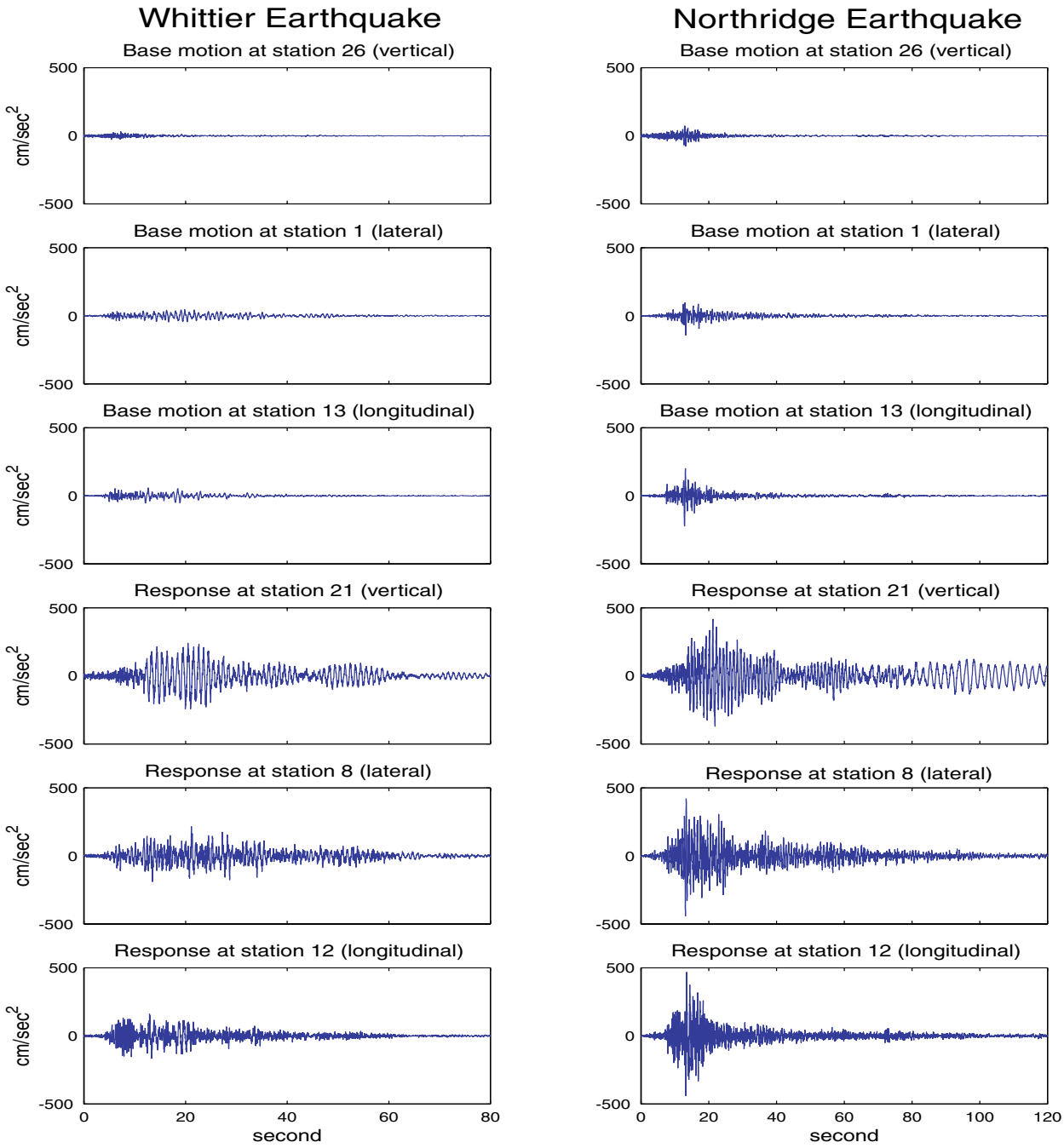

Figure 3: Typical ground motion and structural response time-histories for both earthquakes.

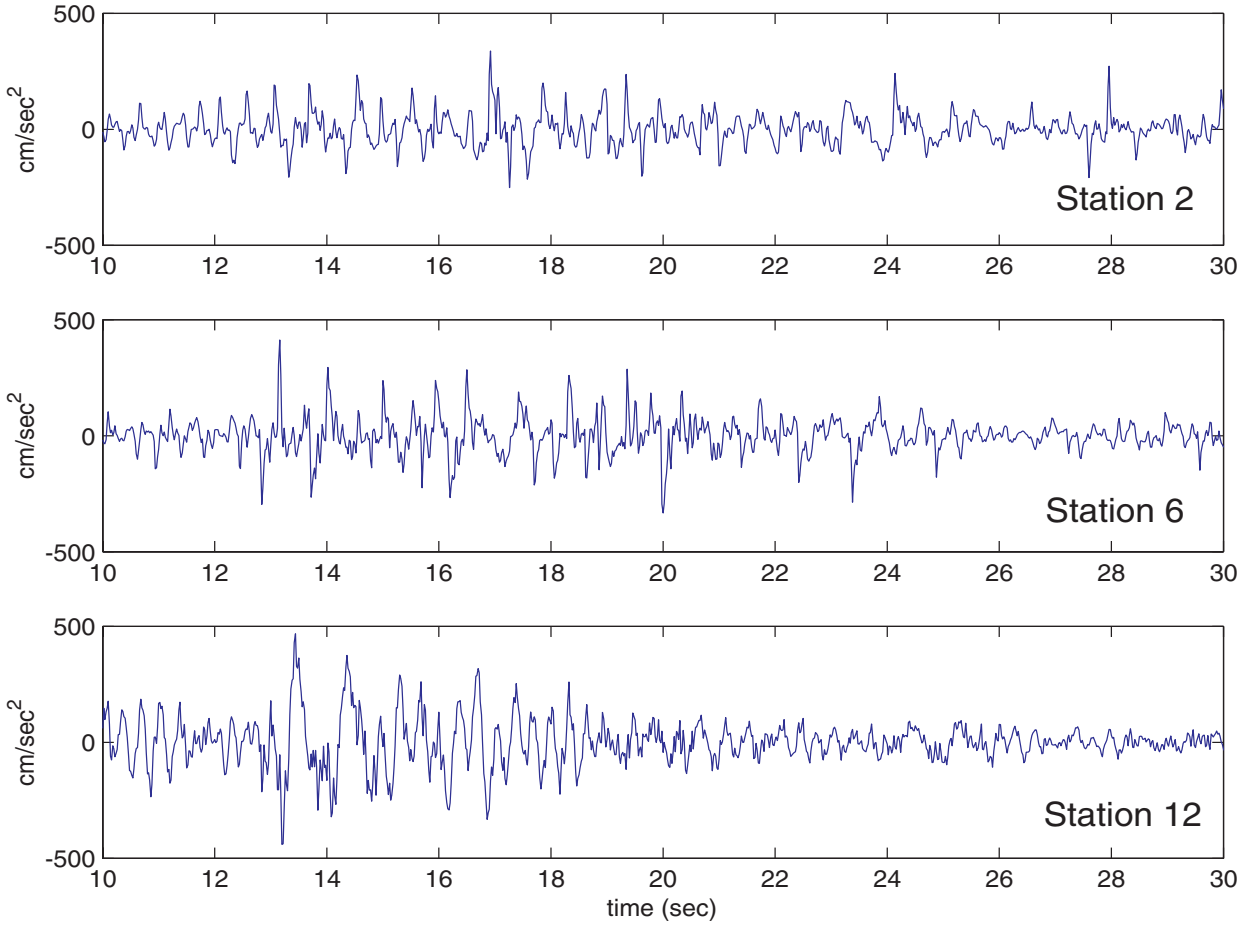

Figure 4: A 20 second window of the measured acceleration response at stations 2, 6, and 12. These accelerograms (particularly those for stations 2 and 6) indicate impulsive accelerations, not seen in any other response records. These locations correspond to the tower-to-deck "wind shoe" connection area, and indicate a significant slipping and banging type of nonlinear behavior.

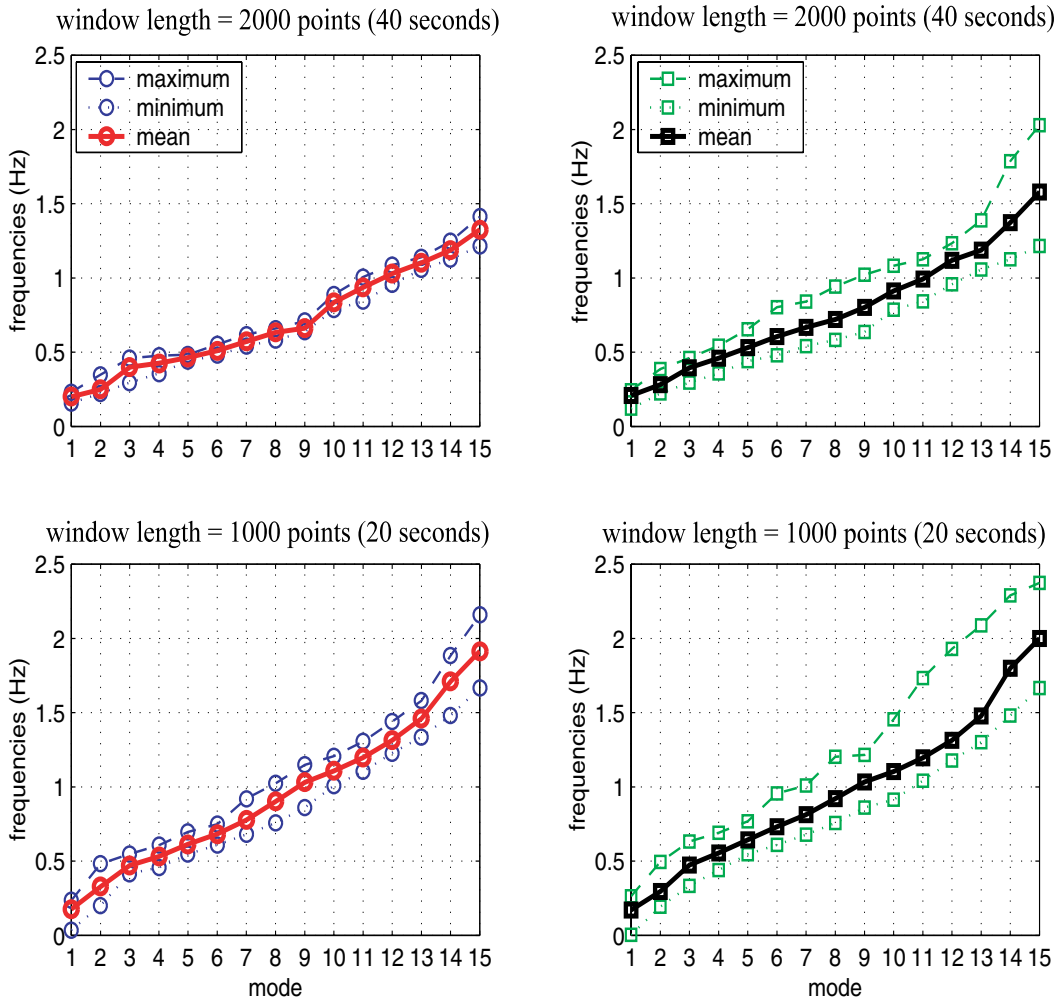

(a) Last 3000 points (60 seconds, approx. $13.2T_1$)

(b) Full history 6000 points (120 seconds, approx. $26.4T_1$)

Figure 5: Variation in maximum, minimum and mean value from (a) the second half history, and (b) the entire records, of unsymmetrically identified modal frequencies for the Northridge earthquake with different window lengths. T_1 is the fundamental period of the identified model for the bridge and was found to be about 4.5 seconds in most of the results.

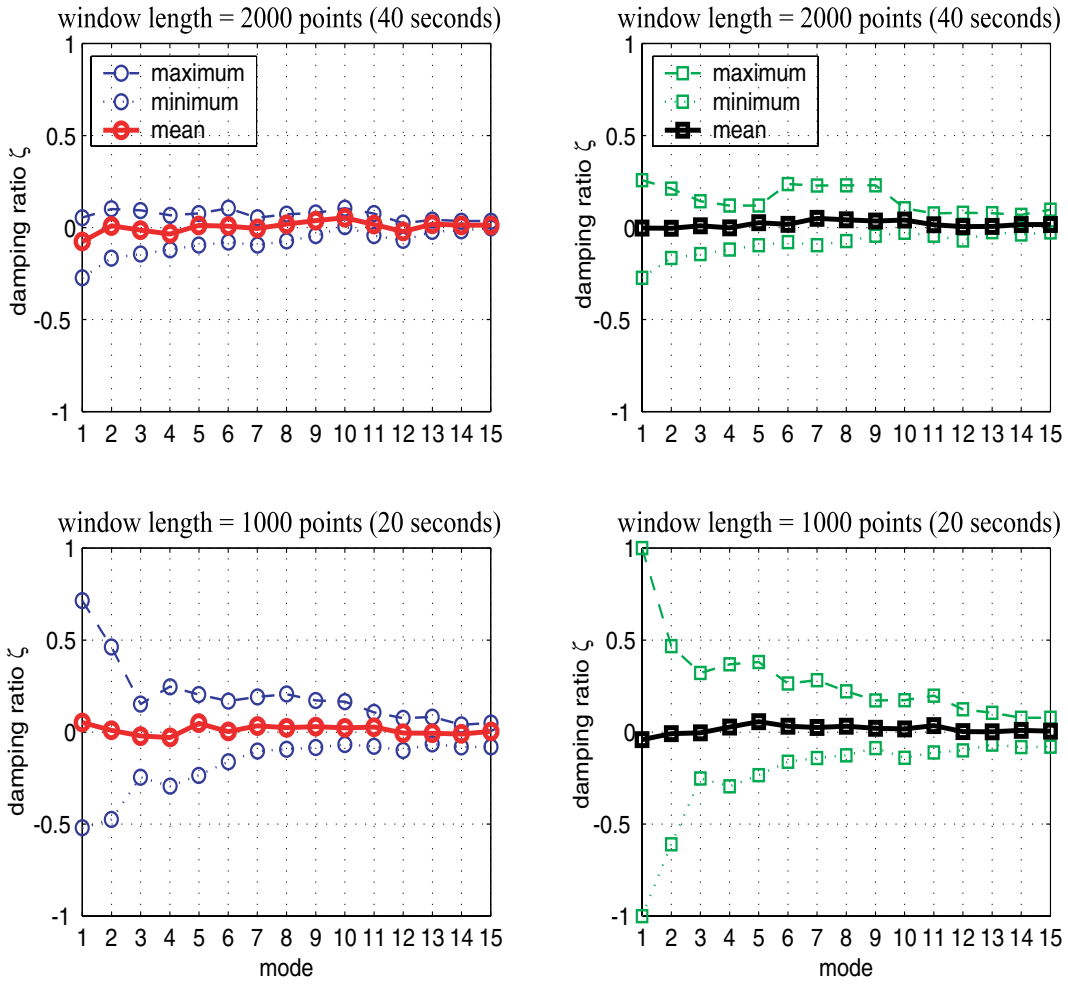

(a) Last 3000 points (60 seconds, approx. $13.2T_1$)

(b) Full history 6000 points (120 seconds, approx $26.4T_1$)

Figure 6: Variation in maximum, minimum and mean value from (a) the second half history, and (b) the entire records, of unsymmetrically identified modal damping ratios for the Northridge earthquake with different window lengths. T_1 is the fundamental period of the identified model for the bridge and was found to be about 4.5 seconds in most of the results.

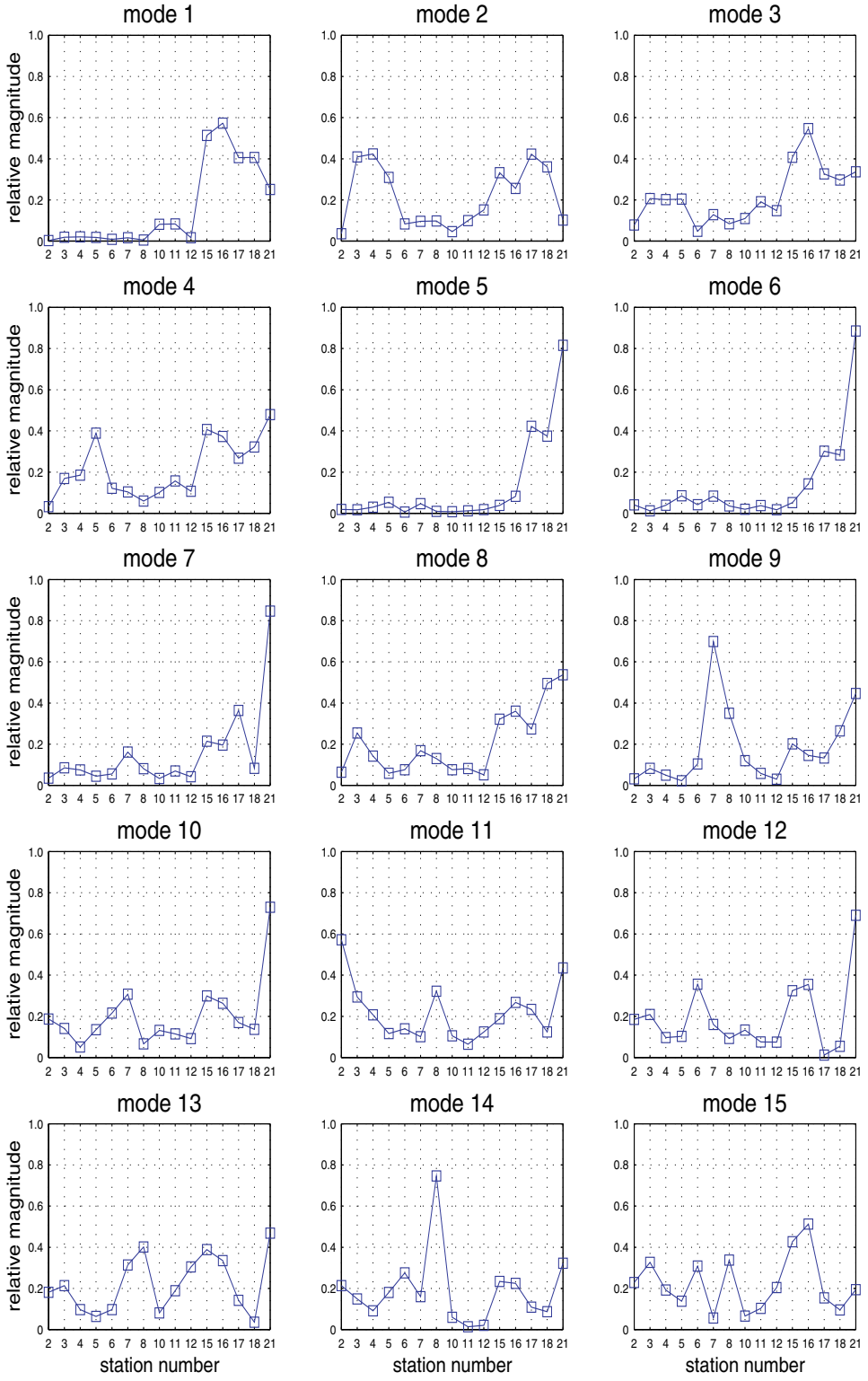

Figure 7: Magnitude plot of a normalized complex mode shapes. The example used here is of the identified mode shapes from the Northridge earthquake with a window covering the last 3000 points in the recorded history.

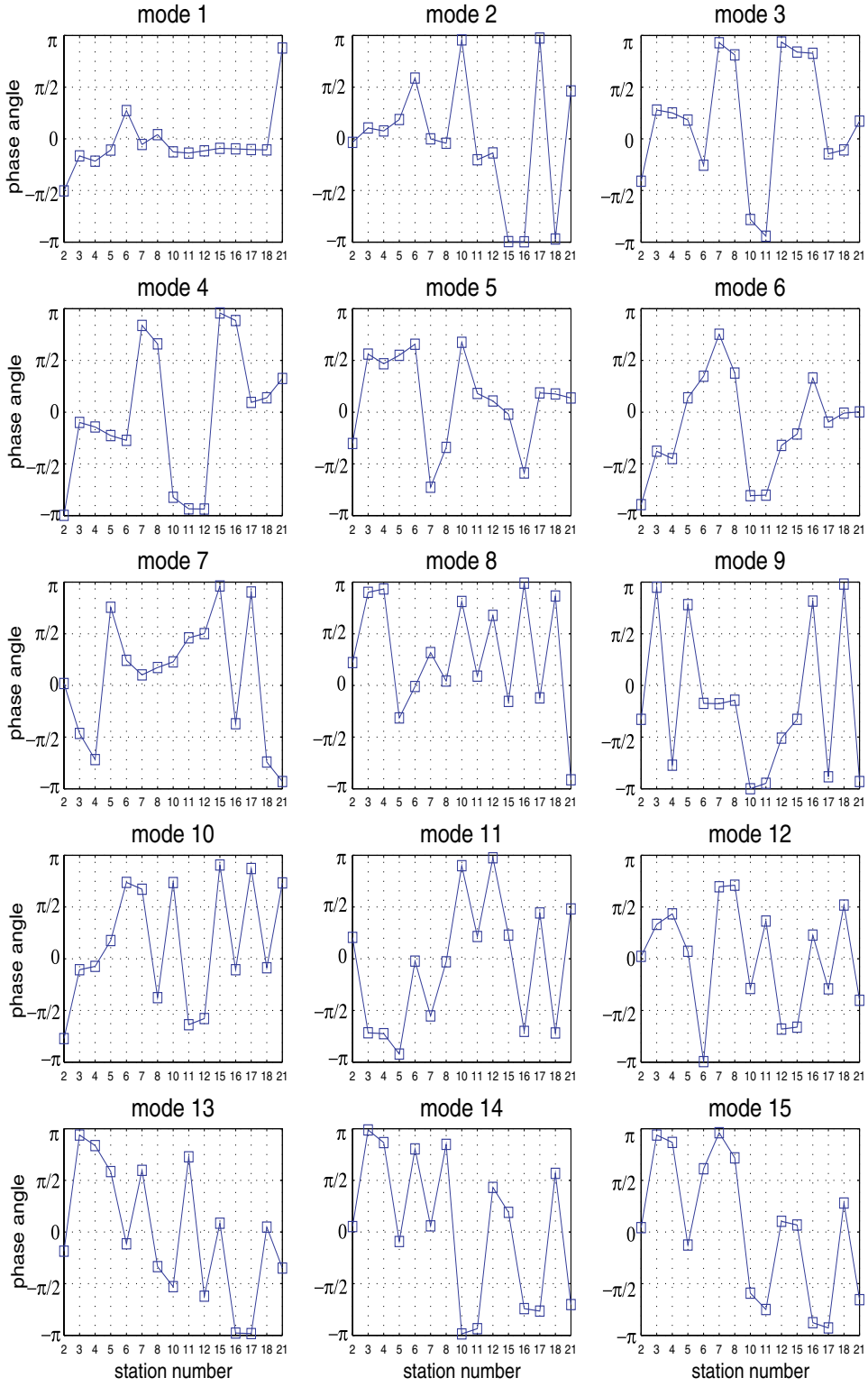

Figure 8: Phase angle plot of the normalized complex mode shapes. The results shown here are from the identified mode shapes for the Northridge earthquake data with a window covering the last 3000 points in the recorded history.

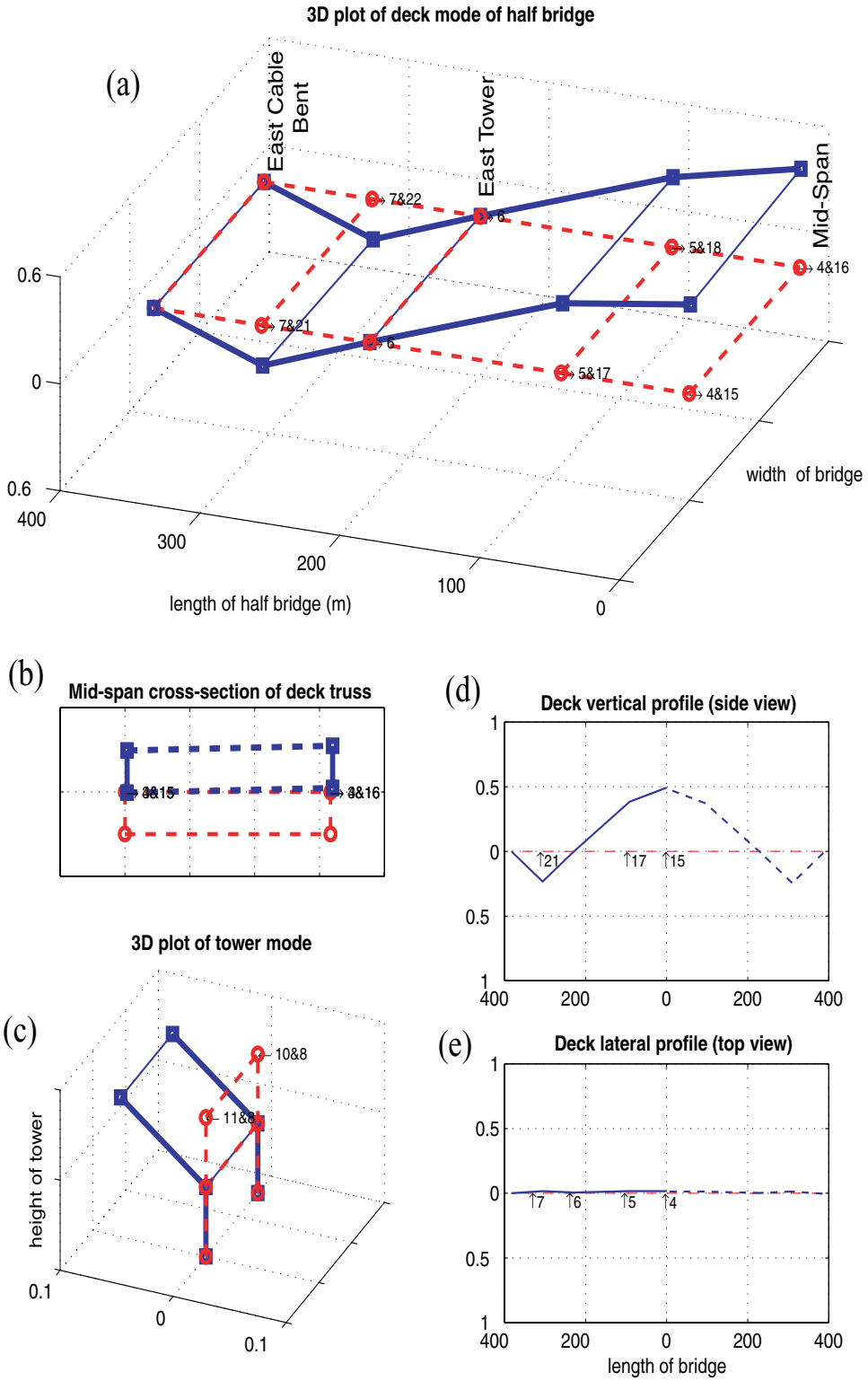

Figure 9: Snap shot of the normalized complex 1st mode. The example used here is from the Northridge earthquake data with a time window covering the last 3000 points in the recorded history.

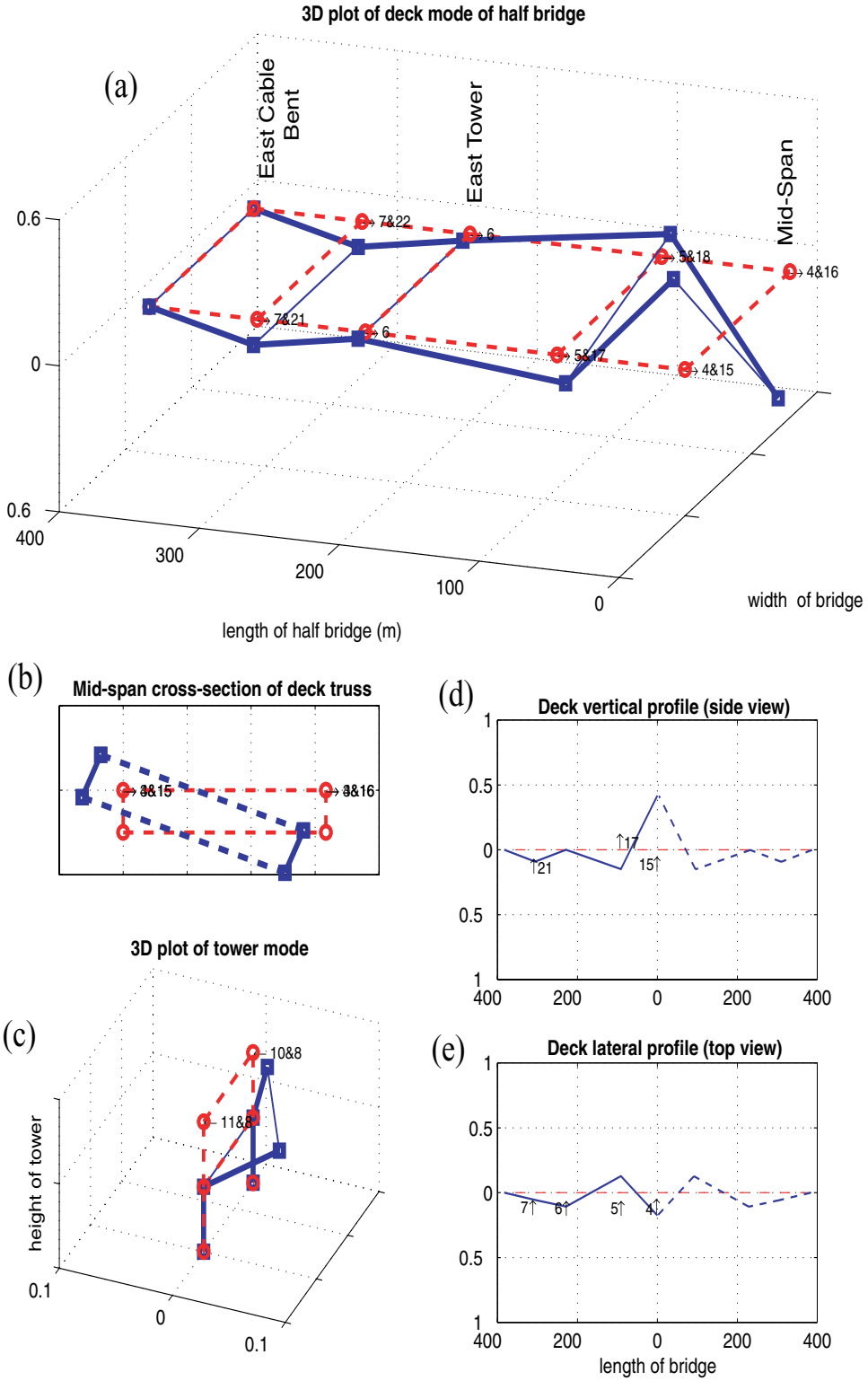

Figure 10: Snap shot of the normalized complex 15th mode. The example used here is from the Northridge earthquake data with a time window covering the last 3000 points in the recorded history.

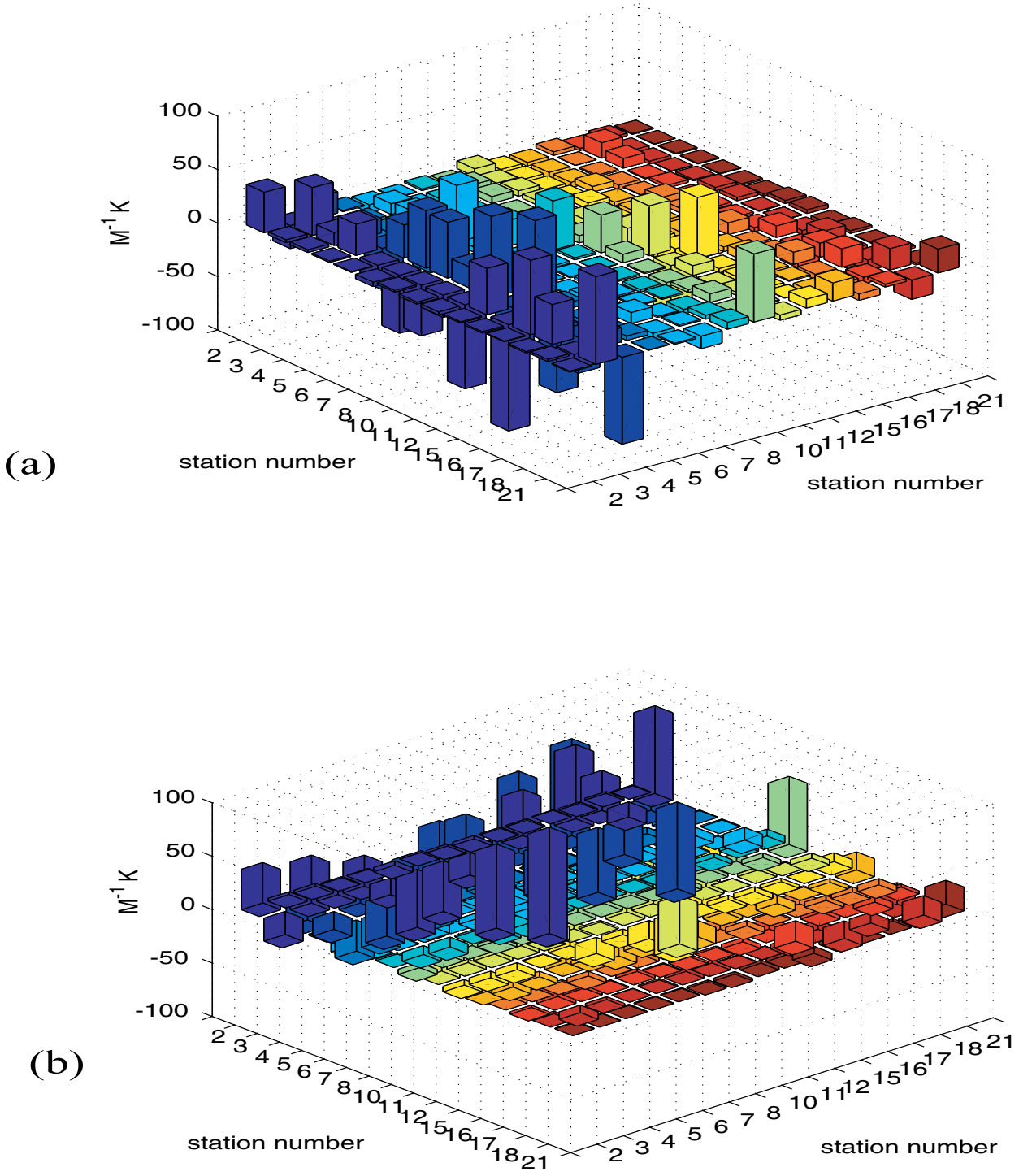

Figure 11: 3-D bar chart (view from above (a) and below (b)) of the identified ${}^{3}\mathbf{A}$ matrix for the Whittier earthquake. The coefficient indices in the ${}^{3}\mathbf{A}$ matrix are related to the original station numbers. The window length used is over the last 3000 points.

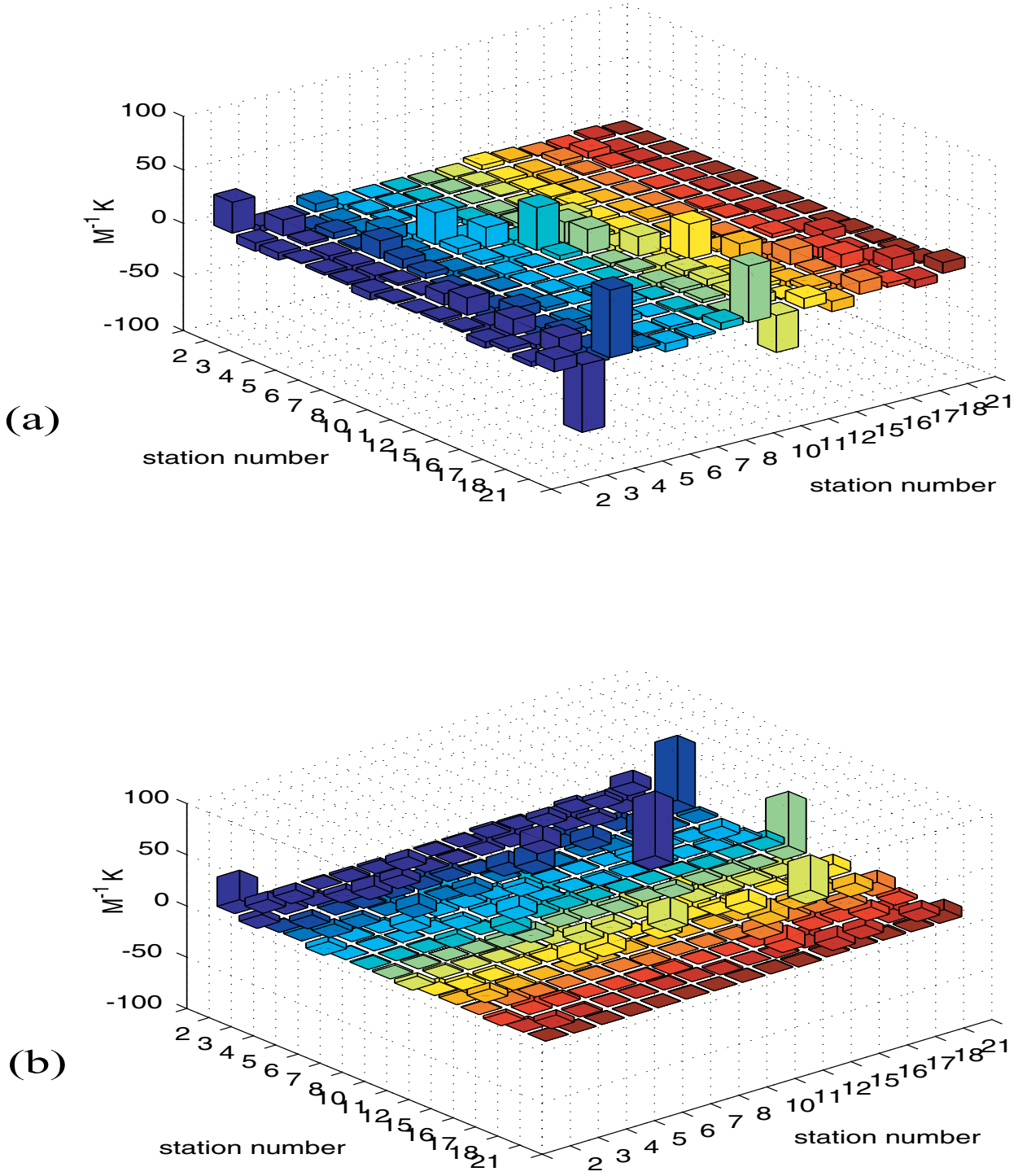

Figure 12: 3-D bar chart (view from above (a) and below (b)) of the identified ${}^{3}\mathbf{A}$ matrix for the Northridge earthquake. The coefficient indices in the ${}^{3}\mathbf{A}$ matrix are related to the original station numbers. The window length used is over the last 3000 points.

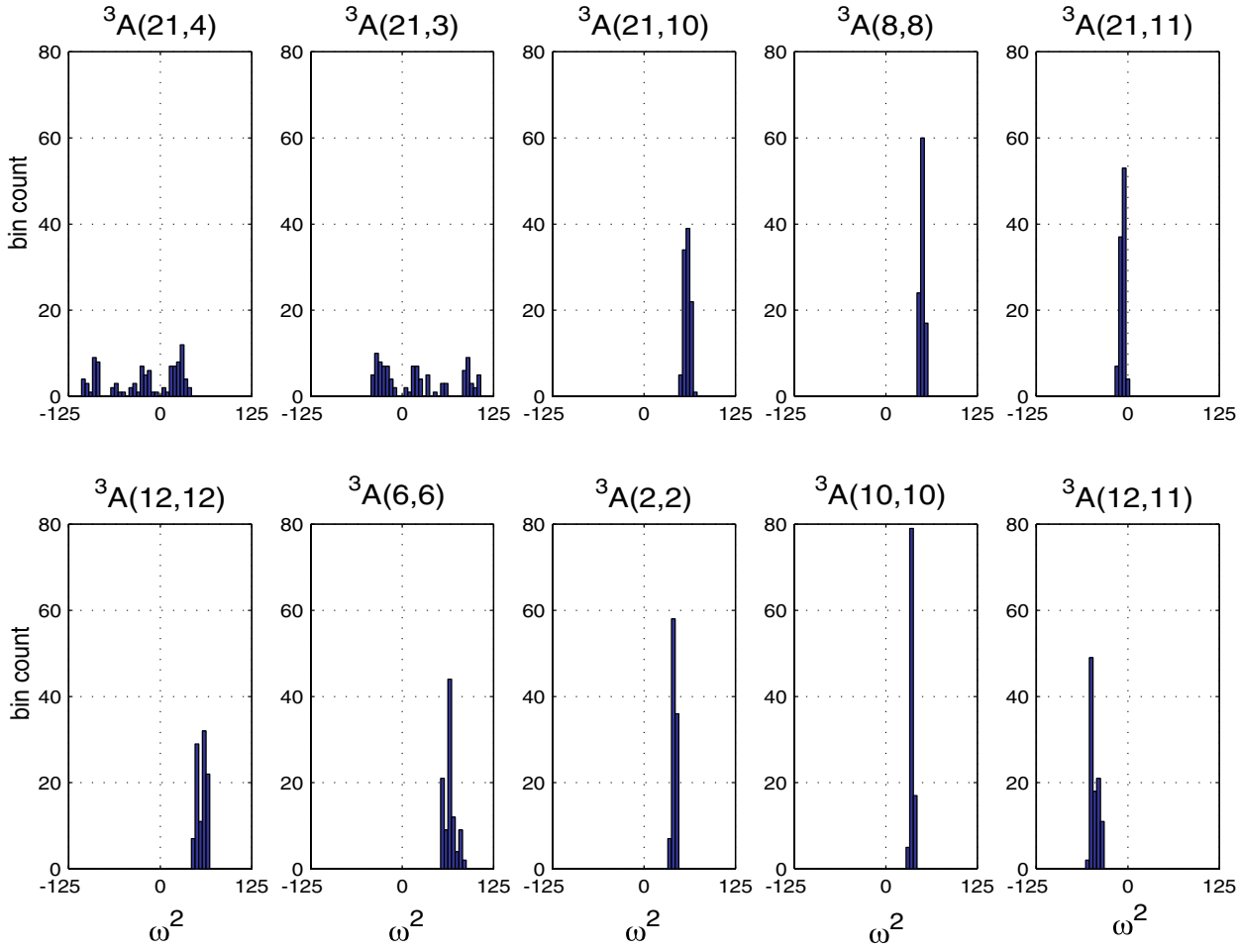

Figure 13: Histograms showing variation in the identified 10 most dominant coefficients (in an absolute sense) in the $^3\mathbf{A}$ matrix for the Whittier earthquake. The variation was produced by performing the identification at numerous shifted windows of length 2000 points over the last 3000 points of measurement time-histories.

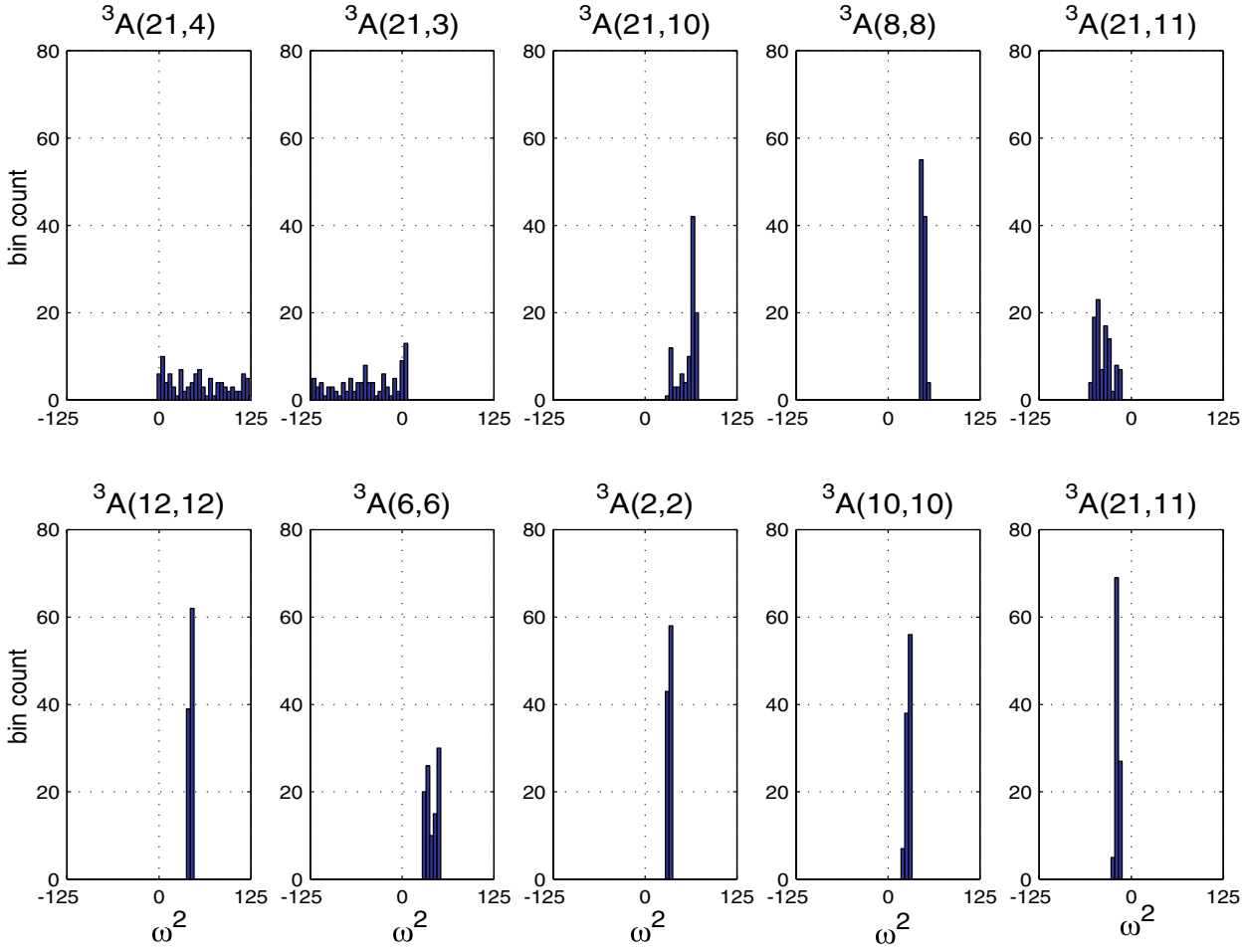

Figure 14: Histograms showing variation in the same dominant coefficients shown in Fig. (13) from the $^3\mathbf{A}$ matrix for the Northridge earthquake. The variation was produced by performing the identification at numerous shifted windows of length 2000 points over the last 3000 points of measurement time-histories.

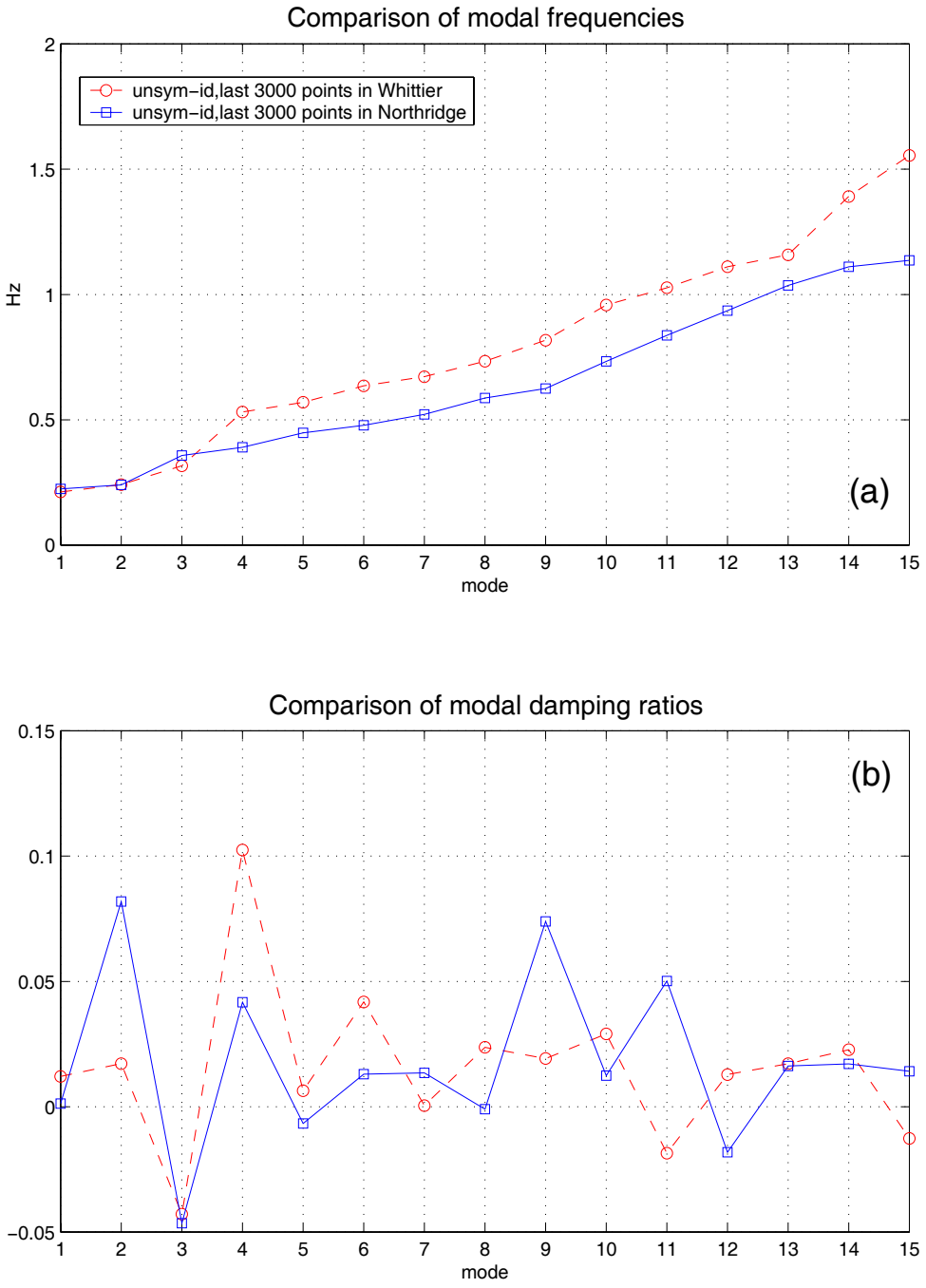

Figure 15: Comparison of modal identified frequencies and damping ratios for the last 3000 points of the time-histories from the Whittier and Northridge earthquakes. Note that care should be taken in drawing conclusions from this because the modes are compared by their number and not by their mode shape.

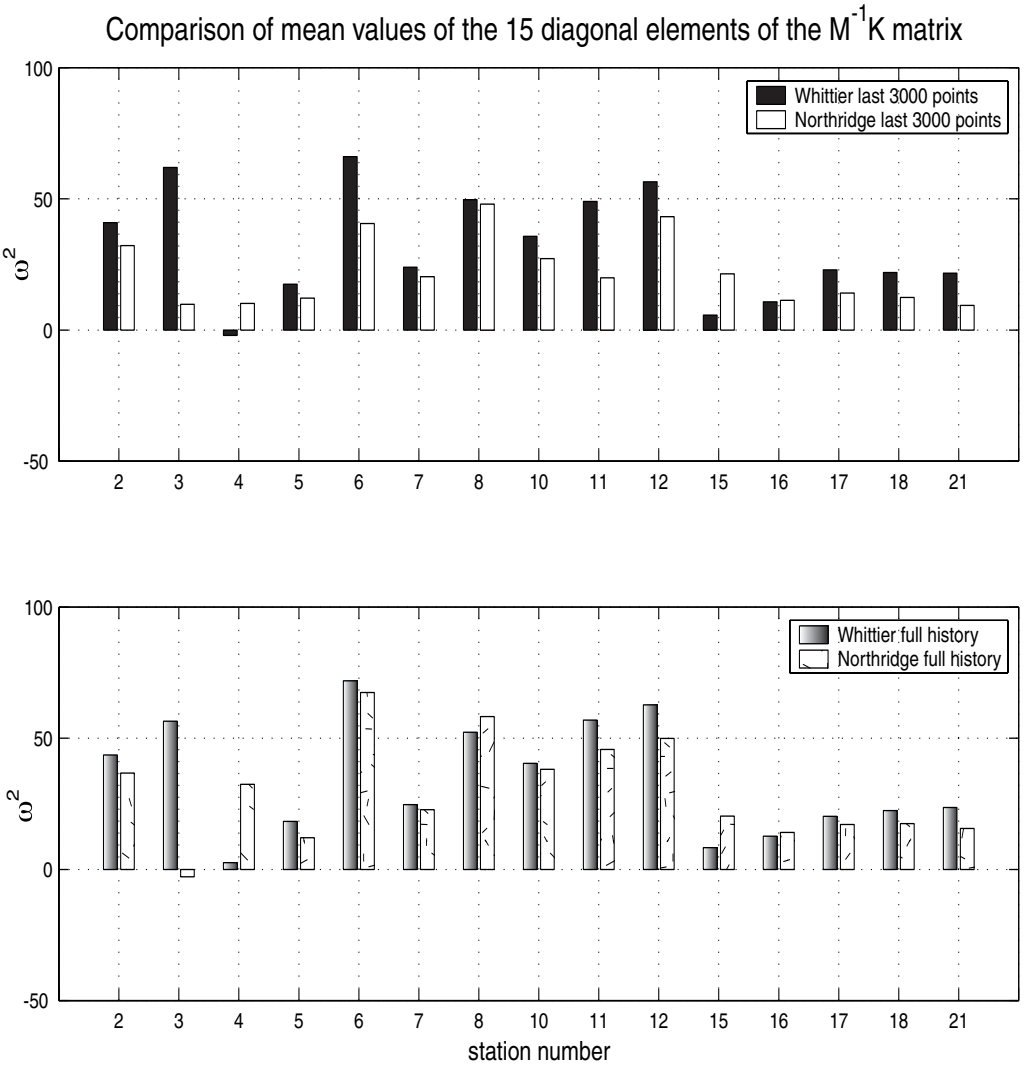

Figure 16: Comparision of the identified mean value of diagonal elements in ${}^3\mathbf{A}$ matrix between Whittier and Northridge earthquake. The variation was produced by performing the identification at numerous shifted windows of length 2000 points over the last 3000 point (top panel) or the full measurement time-histories (bottom panel) for both earthquakes respectively.

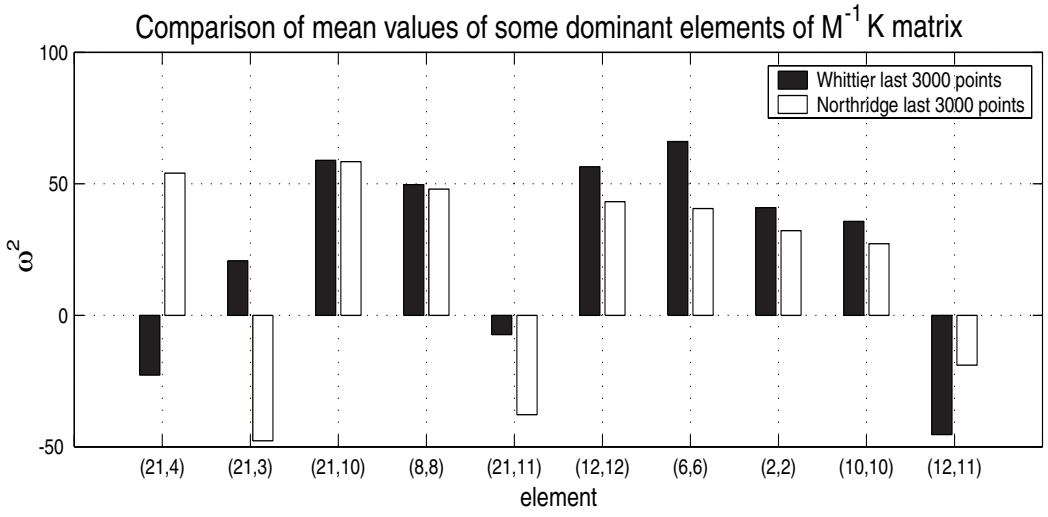

Figure 17: Comparision of the identified mean value of the 10 most dominant elements in ${}^3\mathbf{A}$ matrix between Whittier and Northridge earthquake. The variation was produced by performing the identification at numerous shifted windows of length 2000 points over the last 3000 points for both earthquakes. These are the mean values from Fig. (13) and Fig. (14).

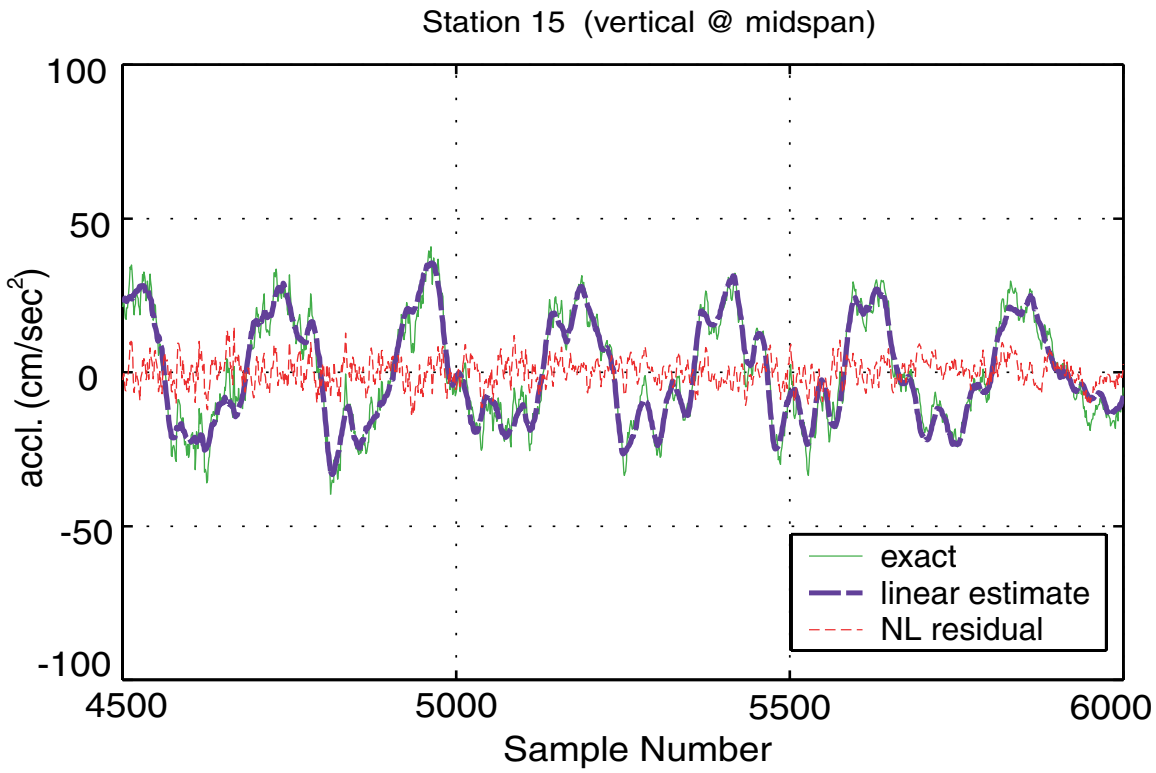

Figure 18: Comparison of the equivalent linear time-invariant system time history fit for the vertical response at Station 15 at the bridge midspan. Note that only the last 1500 points of the 6000 sample record are shown for added resolution. Over the entire earthquake response, the fit error is approximately 20% RMS at this location.

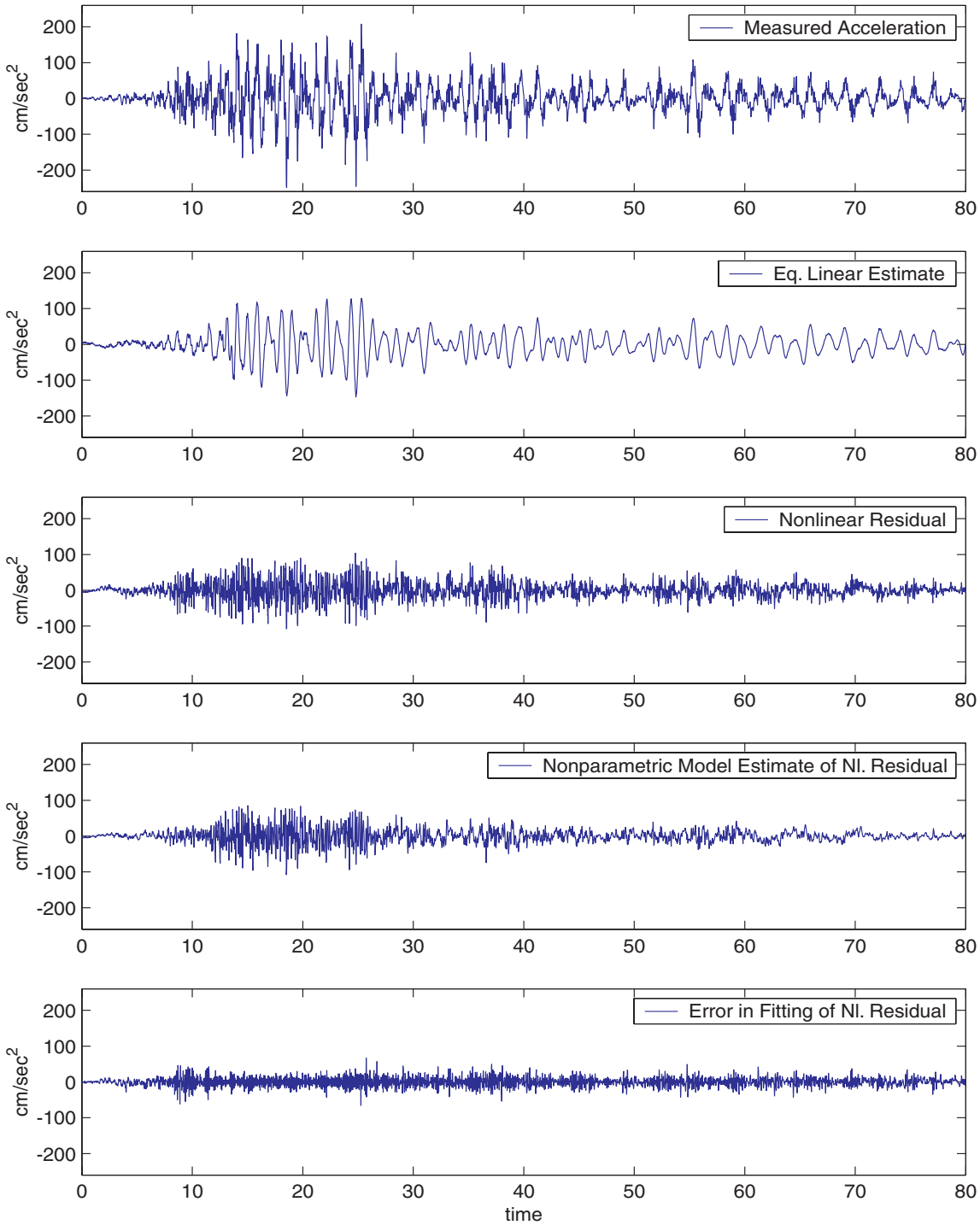

Figure 19: Representative example of the nonlinear residual fitting. In the top panel, the measured station 7 (lateral, side-span) acceleration is shown. Below this is the linear, time-invariant model estimate. The middle panel shows the residual (i.e., the difference of the previous two signals). In the fourth panel the nonparametrically modeled residual is given, and finally at the bottom the remaining total error is shown. For ease of comparison, identical scales are used for all panels.